

**ANALYZING HYDROACOUSTICS OF
CYLINDRICAL SHAPED BODIES CONSIDERING
VARIOUS GEOMETRICAL ASPECTS**



Author

Muhammad Abdullah

Reg. Number

00000397851

Supervisor

DR. ADIL LOYA

DEPARTMENT OF ENGINEERING SCIENCES

PAKISTAN NAVY ENGINEERING COLLEGE

NATIONAL UNIVERSITY OF SCIENCES AND TECHNOLOGY (NUST)

MARCH, 2024

**ANALYZING HYDROACOUSTICS OF
CYLINDRICAL SHAPED BODIES CONSIDERING
VARIOUS GEOMETRICAL ASPECTS**

Author

MUHAMMAD ABDULLAH

Reg. Number

00000397851

A thesis submitted in partial fulfillment of the requirements for the degree of

**MASTER OF SCIENCE
in
Mechanical Engineering**

Thesis Supervisor:

DR. ADIL LOYA

Thesis Supervisor's Signature



**DEPARTMENT OF ENGINEERING SCIENCES
PAKISTAN NAVY ENGINEERING COLLEGE
NATIONAL UNIVERSITY OF SCIENCES AND TECHNOLOGY (NUST)
MARCH, 2024**

THESIS ACCEPTANCE CERTIFICATE

Certified that final copy of MS thesis written by **MUHAMMAD ABDULLAH (00000397851)**, of **NUST - PNEC** has been vetted by undersigned, found complete in all respects as per NUST Statues/Regulations, is free of plagiarism, errors, and mistakes and is accepted as partial fulfillment for award of MS degree. It is further certified that necessary amendments as pointed out by GEC members of the scholar have also been incorporated in the said thesis

Signature: Adil Loya

Name of Supervisor: DR ADIL LOYA

Date: 25/03/2024

Signature (HOD): [Signature]

Date: DEAN ENGINEERING SCIENCE
PA ENGINEERING COLLEGE
PNS JAWHAR
26/03/24

Signature (Dean/Principal): [Signature]

Date: MIRFAN NADEEM
Captain Pakistan Navy
Deputy Commandant
PNS JAWHAR
26/03/24

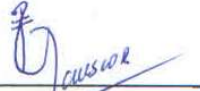
National University of Sciences and Technology

MASTER'S THESIS WORK

We hereby recommend that the dissertation prepared under our supervision by: (Student Name & Regn No.) MUHAMMAD ABDULLAH (00000397851) Titled: ANALYZING HYDROACOUSTIC OF CYLINDRICAL SHAPED TOWED ARRAY SONAR CONSIDERING VARIOUS GEOMETRICAL ASPECTS be accepted in partial fulfillment of the requirements for the award of MS (Mechanical Engineering) degree and awarded grade "A" (initial) AK

Examination Committee Members

1. Name: DR ASIF MANSOOR

Signature: 

2. Name: CDR DR ASGHAR RAZZAQI PN

Signature: 

Supervisor's name: DR ADIL LOYA

Signature: 

Date: 25/03/2024


 Head of Department
 DEPARTMENT OF SCIENCES
 PN ENGINEERING COLLEGE
 PNS JAUHAR

26/03/2024
 Date

COUNTERSIGNED

Date: 26/03/2024


 Dean / Principal
 MIRFAN NADEEM
 Captain Pakistan Navy
 Deputy Commandant
 PNS JAUHAR

Certificate for Plagiarism

1. It is certified that MS Thesis Titled: "ANALYZING HYDROACOUSTIC OF CYLINDRICAL SHAPED TOWED ARRAY SONAR CONSIDERING VARIOUS GEOMETRICAL ASPECTS" by MUHAMMAD ABDULLAH Regn No. 00000397851 has been examined by me. I undertake the follows.

a. Thesis has significant new work as compared to already published or are under consideration to be published elsewhere. No sentence, equation, diagram, table, paragraph or section has been copied verbatim from previous work unless it is placed under quotation marks and duly referenced.

b. The work presented is original and own work of the author (i.e. there is no plagiarism). No ideas, processes, result or words of others have been presented as author own work.

c. There is no fabrication of data or results which have been complied / analyzed.

d. There is no falsification by manipulating research materials, equipment, or processes, or changing or omitting data or results such that the research is not accurately represented in the research record.

e. The thesis has been checked using TURNITIN (copy of originality report attached) and found within limits as per HEC Plagiarism Policy and instructions issued from time to time.



Name & Signature of Supervisor

DR ADIL LOYA
Associate Professor
Thesis Supervisor

Declaration

I certify that this research work titled “*Analyzing hydroacoustic of cylindrical shaped bodies considering various geometrical aspects*” is my own work. The work has not been presented elsewhere for assessment. The material that has been used from other sources it has been properly acknowledged / referred.

A handwritten signature in blue ink, appearing to be 'M. Abdullah', written over a faint horizontal line.

Signature of Student
MUHAMMAD ABDULLAH
2021-NUST-MS-ME-00000397851

Plagiarism Certificate (Turnitin Report)

This thesis has been checked for Plagiarism. Turnitin report endorsed by Supervisor is attached.



Signature of Student
MUHAMMAD ABDULLAH
2021-NUST-MS-ME-00000397851

Signature of Supervisor



Copyright Statement

- Copyright in text of this thesis rests with the student author. Copies (by any process) either in full, or of extracts, may be made only in accordance with instructions given by the author and lodged in the Library of Pakistan Navy Engineering College (PNEC) NUST, Karachi. Details may be obtained by the Librarian. This page must form part of any such copies made. Further copies (by any process) may not be made without the permission (in writing) of the author.
- The ownership of any intellectual property rights which may be described in this thesis is vested in Pakistan Navy Engineering College (PNEC) NUST, Karachi, subject to any prior agreement to the contrary, and may not be made available for use by third parties without the written permission of the aforementioned institute, which will prescribe the terms and conditions of any such agreement.
- Further information on the conditions under which disclosures and exploitation may take place is available from the Library of Pakistan Navy Engineering College (PNEC) NUST, Karachi.

Acknowledgements

First, I want to express my gratitude to Allah Almighty, who is always with us and The Holy Prophet (PBUH), who is my ideal, a sign of direction, and a source of knowledge for us, deserves all the praise. My parents and my wife, who hoped for my success and supported me at all times, deserve my gratitude.

Furthermore, I would like to thank

Dr. Adil Loya, My supervisor, helped me in understanding the STAR CCM+ software and simulation work of the thesis. His kind supervision has improved my research abilities. I gained a lot of CFD knowledge under his supervision and direction. His professional and friendly supervision has greatly enhanced my performance. Under his supervision and guidance, I have greatly enhanced my research skills and acquired valuable knowledge.

Cdre Dr Shafiq ur Rehman, My co-supervisor from MTC, for providing me opportunity to work on the project which will be beneficial to Pakistan Navy in future. He guided me throughout this research work and assisted me in the completion of this research work.

Dr. Asif Mansoor & Cdr Dr Asghar Razzaqi PN, My GEC members who helped me to carry out this research, their critical thanking and observations and continuous guidance has helped me to ascertain concepts better.

Ghulam Mustafa, My uncle and also my teacher, who inculcated such traits in my personality which proved very beneficial for the successful completion of this dissertation.

Dedicated to my Supervisor, beloved parents, my wife and specially to my uncle Ghulam Mustafa for his unwavering guidance, motivation and teachings since my childhood which led me to this remarkable achievement.

Abstract

The maritime industry has significant challenges on several fronts, including commercially, militarily, and ecologically; one of these challenges is the prediction and reduction of noise generated by underwater activities. The three main types of underwater noise for submerged bodies are machine, flow, and propeller noise. The primary source of the underwater noise emitted from these bodies is flow noise, particularly at elevated flow velocities. Variations in the hydroacoustic characteristics are seen because of altered geometric factors. First, the formation of various hydroacoustic properties because of diameter change is analysed in this work. Then, the models and techniques used for turbulence modelling and computation fluid dynamics (CFD) have been reviewed, and the advantages and disadvantages of each turbulent model are assessed. Several hybrid methods for hydroacoustic modelling comprising CFD plus acoustic findings, such as Reynolds-averaged Navier-stokes (RANS) with Ffwoes Willaim Hawking equation (FWH) and large-eddy simulations (LES) with FWH have been analysed to ascertain hydroacoustic trends w.r.t diametrical changes. Models having diameter of 10, 25 and 50 mm were considered. Simulations were carried out on 2 different velocities 3.05 m/sec and 5.05 m/sec. Results obtained from LES were considerably better than RANS models w.r.t acoustic depiction and same were then utilized for analysis with respect to diameter reduction. Decrease in acoustic noise has been observed with reduction in diameter of selected models. Efficacy of diameter reduction and estimation of flow noise levels/ patterns w.r.t change in diameter of cylindrical shaped underwater bodies is mainly assessed in this research work.

Keywords: Hydroacoustic, Flow Noise, Ffwoes Willaim Hawking, Large-eddy simulations, Reynolds-averaged Navier-stokes

Table of Contents

Declaration	i
Plagiarism Certificate (Turnitin Report)	v
Copyright Statement	vi
Acknowledgements	vii
Abstract	ix
Table of Contents	x
List of Figures	xiii
List of Tables	xiv
Nomenclature	xv
CHAPTER 1: INTRODUCTION	1
1.1 Problem Statement	2
1.2 Objective of the Study	3
1.3 Thesis Anatomy.....	3
CHAPTER 2: Literature Review	5
2.1 Acoustics Methods for Hydroacoustic Noise Finding from Underwater Bodies:.....	5
2.2 Turbulence Flow Modeling Methods for Hydroacoustic Noise Finding from Underwater Bodies:	7
2.2.1 RANS	9
2.2.2 k- ω & k- ϵ Model	9
2.2.3 Shear-Stress Transport (SST) Model	10
2.2.4 Advanced Eddy Viscosity Model.....	10
2.2.5 RN Stress Model	11
2.2.6 LES.....	12

2.2.7 DNS.....	13
2.2.8 DES	13
2.3 Using Acoustic Analogies and Turbulence Models for CFD in Cylindrical Bodies Considering Different Factors.....	15
2.4 Computational Fluid Dynamics (CFD) Simulations	22
CHAPTER 3: METHODOLOGY	25
3.1 Pre-Processing.....	25
3.1.1 Grid Generation.....	25
3.1.2 Prism Layer Mesher	27
3.1.3 Extruder Mesher.....	27
3.2 Mathematical Modeling	28
3.3 Post Processing.....	32
3.3.1 Reports	32
3.3.2 Monitors	33
3.3.3 Scenes.....	33
3.4 Fast Fourier Transform (FFT) Plots	34
Chapter 4 Validation	35
4.1 Drag Validation of DARPA Suboff:	35
4.1.1 Mesh Independence Study	36
4.1.2 Acoustics Validation with results of H. Yao et al., 2017.....	38
4.2 Acoustics Validation with K Karthik et al., 2020 on Cylindrical shaped under water body.....	40
4.3 Outcomes of validation work:	41
Chapter 5 Simulation.....	42
5.1 Modeling	42
5.2 Computational Domain	43

5.3 Boundary Conditions.....	44
5.4 Physics Conditions	45
5.5 Meshing.....	45
5.6 Virtual Hydrophones	48
Chapter 6: Results & Discussion	49
Chapter 7: Conclusion and Future Prospect.....	55
7.1 Conclusion.....	55
7.2 Future Prospect.....	56
References.....	57

List of Figures

Figure 2.1: Turbulence models Comparison for Hydroacoustic Noise Finding.....	26
Figure 3.1: Grid generation (structured and unstructured mesh)	40
Figure 3.2: Mesh types a) Hexahedral Mesh b) Tetrahedral Mesh c) Polyhedral Mesh.....	41
Figure 4.1: Top View of DARPA Suboff	36
Figure 4.2: Mesh View of DARPA Suboff.....	37
Figure 4.3: Scaler scene (Velocity magnitude) of DARPA Suboff.....	37
Figure 4.4: Calculated DARPA Suboff Drag.....	37
Figure 4.5: Flow noise of the DARPA Suboff by (H. Yao et al., 2017) using FW-H and BEM.....	38
Figure 4.6: Calculated Flow noise of the DARPA Suboff using FW-H (CFD).....	39
Figure 4.7: Comparison of Flow noise of the DARPA Suboff with results of H. Yao et al., 2017.....	39
Figure 4.8: Depiction of underwater body in domain.....	40
Figure 4.9: Comparison with obtained Results of K Karthik et al., 2020.....	41
Figure 5.1: Research Methodology.....	42
Figure 5.2: Under water cylindrical shaped bodies with diameter of 50, 25, 10 mm.....	43
Figure 5.3: Domain of the underwater cylindrical shaped body	44
Figure 5.4: Refined Cylindrical Domain of underwater cylindrical shaped body.....	44
Figure 5.6: Mesh Depiction bodies with 10, 25- & 50 mm diameter.....	46
Figure 5.7: Mesh of the refinement zones and surface from top.....	46
Figure 5.8: Mesh inside of the domain for underwater cylindrical shaped body	47
Figure 5.9: Prism layers close to the surface of the body.....	47
Figure 5.10: Visualization of the virtual hydrophones around the body.....	48
Figure 6.1: Sound Pressure Level Vs Frequency Plot at 3.05 m/sec (Using LES Model)	50
Figure 6.2: Sound Pressure Level Vs Frequency Plot at 5.05 m/sec (Using LES Model)	50
Figure 6.3: Scaler Scenes Comparison (Velocity Function)	51
Figure 6.4: Scaler Scenes Comparison (Pressure Function)	52
Figure 6.5: Residuals in Continuity, X, Y, Z momentum.....	52

List of Tables

Table 2.1: Evaluation of Numerous Turbulence Models Benefits and Shortcomings.....	14
Table 2.2: Drag coefficient and Strouhal number Comparisons for Circular Cylinders with Change in Dimensions in Medium of Air and Water.....	22
Table :4.1 Mesh density w.r.t base size.....	36
Table 4.2: Comparison of the CFD results with the experiment.....	37
Table 5.1: Boundary Conditions.....	40

Nomenclature

ADCP	: Acoustic Doppler Current Profiler
BEM	: Boundary Element Method
CAA	: Computational Aero Acoustics
CFD	: Computational Fluid Dynamics
dB	: Decibel
FFT	: Fast Fourier Transform
FW-H	: Ffowcs Williams-Hawkings
OASPL	: Over All Sound Pressure Level
RANS	: Reynolds Averaged Navier Stokes
RF	: Radio Frequency
SEL	: Sound Exposure Level
SONAR	: Sound Navigation and Ranging
SPL	: Sound Pressure Level
TBL	: Turbulent Boundary Layer
TKE	: Turbulent Kinetic Energy
UUV	: Unmanned Underwater Vehicle

CHAPTER 1: INTRODUCTION

Underwater noise from immersed bodies turns out to be a great concern that is getting much attention. The environmental noise pollution that it causes and its detrimental effects on aquatic animals are two of the most crucial matters that have emerged as a direct consequence of increased noise levels [1]. Boundary-layer pressure variations in turbulent flows produce fluid-induced structural and hydrodynamic noise.[2] Eddies in turbulent flow cause the body surface to vibrate flexibly, which makes the structural noise caused by flow. When it comes to flow-induced structural noise problems, the vigorous interface amid structures and the fluid adjoining them are of particular matter [3]. Other significant aspects of flow-induced structural noise include transmission, reflection, wave propagation [4, 5], the use of efficient materials with special properties [6-8], and the use of metamaterials [9-11]. Hydrodynamic noise refers to any phenomenon in which flow areas cause pressure instabilities. The leading causes of the hydrodynamic noise are rotating eddies' centrifugal forces, Coriolis forces, and microscopic stagnation pressures. The hydrodynamic noise produced by bluff bodies is extremely interesting for industrial and ecological purposes. The parts of the promontory body have been applied frequently in seaward structures, submarines, and undersea applications like wires, wires, and pipelines. Because of their wide scale of uses in maritime, studying hydrodynamic noise from cylindrical bodies with different segments is of utmost significance. A thorough comprehension of the mechanisms by which submerged bodies generate noise is crucial for developing methods of mitigating this noise's propagation into the far field. Understanding the physics behind noise production is of particular interest in the context of underwater noise [12, 13].

Numerous engineering applications involve various bluff bodies, such as square, circular, or rectangular cylinders. Despite having simple geometries, these cylinders interact with the flow field more complicatedly. Unwanted noise levels are produced due to this complicated phenomenon, which includes velocity variation, vortex development, flow separation in the wake, and shear-layer unpredictability. Because bluff bodies experience significant flow separation over a substantial portion of the body, various flow structures develop in their path. Even though the bluff bodies' geometry has a remarkable impact on the dynamic forces that are generated because of their distinct flow forms, the process of vortex generation is geometrically analogous [14, 15]. As a result, different bluff body geometries produce other acoustic characteristics. Due to its

incredibly complex structure, it is challenging to determine the noise produced by a glutinous flow over a cylinder at high and moderate Reynolds numbers. There are several difficulties with the stream field around a cylinder, including flow splitting brought on by a negative pressure slope and the flaking of vortices due to the interface of split shear layers. Additionally, the calculation of flow noise is complicated by complex physical phenomena, such as propagation and noise production, multiple sources, dissipation, and dispersion. These factors make for a variety of unique challenges. The issue must be examined over a considerable distance to study acoustic wave propagation. Sound computation requires an immediate resolution of the compressible flow calculations. This is because the sound is characterized as a force variation circulating at a predetermined speediness based on the isentropic flow hypothesis. On the other hand, water behaves like an IF, and the hydrodynamic noise field is assessed underneath the in-compressible flow supposition. The incompressibility hypothesis forbids any spread phenomena as the sound broadcast speed approaches infinity [16-18].

Numerous numerical approaches have been put out since the inception of computational aeroacoustics, each of which attempts to address the difficulties provided by the studied problems to compute the radiated sound effectively and precisely. For the simulation of flow noise issues, it is necessary to consider acoustic inefficiency, energy disparity, dispersion, length scale disparity, preservation of various characters, and challenges resulting from nonlinear wave phenomena. Therefore, solving the RANS directly for mathematical hydroacoustic is physically impossible. A hybrid method that unites a hydrodynamic fluid convergent thinker with a hydrodynamic noise problem solver can be used to determine the noise. In the hybrid method, the flow amounts are first calculated as sound sources. Integral formulations evaluate noise propagation in the far field. An acoustic resemblance can solve the acoustic problem, while a turbulence model can be used to determine the flow field. Using aeroacoustics comparisons, hybrid systems in computational aeroacoustics separate the flow from the acoustic calculation [19]. In this paper, there is a discussion about models and approaches used for hydroacoustic characteristics, hydroacoustic noise for cylindrical objects, has been reviewed. Also, the validation of the outcomes in other research has been overviewed in the subsequent sections.

1.1 Problem Statement

The rise in demand for towed array SONAR systems can be attributed to advancements in defense operations, increasing focus on developing robust anti-submarine warfare (ASW)

capability and fleet expansion initiatives, and high military spending for research and development activities. My focus in this research work is to analyze various geometrical aspects which effects the flow noise of Towed Array SONAR. The impact of change in geometric dimensions will give insight into future fabrication in this domain. Innovative designs that keep up with the need for increased efficiency and sustainability are made possible by such approaches, which allow quicker and more robust research of the design space, with or without the aid of optimization tools, as well as lowering the cost of operating assets and components. Use of numerous turbulence flow models along with hybrid models for hydroacoustic noise prediction will be used during this work. Furthermore, the use of software tools such as STAR-CCM+ will also be considered for gathering essential data for comprehending how geometric factors affect the hydroacoustic properties of cylindrical structures.

1.2 Objective of the Study

Analyzing efficacy of diameter reduction & estimation of flow noise levels for cylindrical shaped under water bodies and estimation of flow noise levels/ patterns for cylindrical shaped bodies.

1.3 Thesis Anatomy

Chapter 1: This chapter includes a brief introduction to the importance of underwater vehicles, hydrodynamics, and a comparison of experimental and CFD methods. Also, the objectives and approach to this research study are being discussed

Chapter 2: This chapter includes a literature review on relevant, well-timed research on hydroacoustic analysis of underwater bodies their geometrical aspects and synthesize it into a cohesive summary.

Chapter 3: In this chapter, methodology used to achieve the major goals of this study is presented in. Additionally, it provides a broad introduction to the study's software tools. Moreover, emphasizes the governing equations and a step-by-step approach to the model creation theories.

Chapter 4: This chapter renders an overview of the process of validating and verifying the outcomes (hydrodynamic and hydroacoustic validation) obtained from executed analyses.

Chapter 5: The methodology of the simulations that were performed are reported and analysed is explained.

Chapter 6: This chapter includes detailed results achieved during simulations and brief discussion on achieved results

Chapter 7: In this Chapter conclusion is drawn on basis of research work and simulation. Moreover suggestions for more research and recommendations as future prospect is written.

CHAPTER 2: Literature Review

2.1 Acoustics Methods for Hydroacoustic Noise Finding from Underwater Bodies:

The compressible Navier- Stokes equation (NSE) is converted into an accurate heterogeneous wave equation in Lighthill's (LH's) first proposed acoustic analogy. LH's equation expresses a broad wave equation regarding fluctuating density [20]. About the limits, no presumptions are made in their local form. While this is the case, with a small Mach number approximation of the supply term, satisfactory results can be obtained by solving LH's wave equation with sufficient boundary conditions [21]. However, Light hill suggested utilizing Green's function for free field radioactivity to work out the wave equation. This ignores bodies and resonators in the vicinity of the sources and reflection, absorption, dispersion, and diffraction by solid boundaries. Within LH's theory's integral resolution framework, Curle examined the impacts of surfaces at rest [22]. Surface dipole distributions are the same as surfaces at rest. FWH expanded Kirchhoff's formula and simplified the integral mixture to account for random transporting bodies in the source field [23]. The hypotheses of Ribner and Powell were based on comparing an incompressible flow (IF) with a somewhat compressible flow in which vorticity sources predominate [24, 25]. However, Howe and Mohring conducted additional research with vortex sound [26, 27]. According to Goldstein's recently expanded acoustic analogy, the NSEs can be represented as a series of linearized Euler equations (LEEs) [28]. Similarities to aeroacoustics are effective at computing noise radiation. Fundamental presumption constrains these techniques' implementation, such as small Mach number flows or efficient acoustic sources. Acoustic compact sources suggest that the specific dimension of the source's generating acoustics is small-scale associated with the produced wavelength. Furthermore, since the sources rely on the resolution of the equations, there is uncertainty in the acoustic analogies [29, 30].

The second method relies on the direct computation of acoustics. It flows, which resolves compressible preservation equations and yields the combined effect of flow and acoustics (every so often, also called Direct Noise Computation (DNC)) [31]. Since few model suppositions are required to compute acoustics and flow with one simulation, this approach is more general than acoustic analogies. But the necessary resources are comparatively significant in the limit of low-

down Mach values. Preferably, this approach is applied in the medium-high-ranking-level-Mach number range. This technique has been widely applied to compute applications in jet noise and validate acoustic analogies over the years. These techniques are still in use today, even in the low-down; the linearized Euler equation has undergone modifications over time to ensure that only acoustic waves are transmitted Mach number scheme [32]. To directly solve the flow and acoustic field, the Lattice Boltzmann method has recently grown in popularity. The use of this technique in acoustics ranges from air-frame noise to models of landing gears, the automobile sector, and industrial applications [33]. The 3rd method for calculating aeroacoustics is to decompose the field effects systematically. The specific flow field is divided into two parts: an acoustic part and a fluid dynamic to aeroacoustics comparisons, this acoustic component is also present within the flow sphere, and as a result, in the acoustic near field, The linearized Euler equation has undergone modifications over time to ensure that only acoustic waves are transmitted The field constraints are divided into a fluctuating and temporal-mean component developing the LEE. The important aeroacoustics source conditions on the LEE's momentum equation have been investigated [34]. The linearized Euler equation has undergone modifications over time to ensure that only acoustic waves are transmitted. An alternative filtering method was suggested in [35] for a uniform flow field. The acoustic modes' LEE-derived properties screen the wave equations' resource components rather than filtering the flow field.

To decompose the principal fluctuating pressure variable quantity of LH's analogy into an acoustic pressure and a pseudo-pressure element, Ribner created his dilatation equation. Pope and Hardin developed their acoustic/viscous splitting approach expansion around the incompressible flow (EIF), where they added a concentration adjustment [36]. The pulsing sphere and the stream confirm EIF over a rectangular space. The initial EIF formulation was criticized for its consistency issues. For non-isentropic flows, Shen et al. modified this approach [37]. The round cylinder and the pulsing sphere are used to validate their extent. An economical and verified method for aerodynamic/acoustic splitting that uses a noncompact source region was proposed by Simon et al. [38]. By use of a Mach number expansion, this new application of the EIF approach is systematically derived. In various versions and complexity, Schroder and Ewert used a somewhat different methodology for an APE generation [35, 39]. APE-1 is a generic formulation that uses velocity and pressure perturbations to describe the entire system. An unsteady IF simulation is employed in combination with the APE-2 interpretation. The newly proposed APE-3 system is

identical to the APE-1 system, which also relies on agitated overall enthalpy. This interpretation has one benefit over the APE-1 in that the source terms do not need to be determined by solving Poisson's equation. The APE-4 alternate of the performance is assembled on the APE-1 structure, making it simple to compute the sources using a compressible flow model [40]. Kaltenbacher and Huppe created the perturbed convective wave equation as a mathematically effective re-interpretation of the APE-2 system (PCWE) [41].

Munz and colleagues proposed an alternate method of constructing the acoustic perturbed equations by Mach number grading. The overall derivative of the IF pressure perturbation performs the function as an essential source term in the LEE created by this hypothesis, which is included in the squeezable Euler equations [42]. Roeck and Desmet debated whether an acoustic/aerodynamic splitting method based on Helmholtz breakdown was necessary. The field is first divided into a fluctuating part and a mean flow field to derive the LEE [43]. The fluctuating part is further divided into acoustic and aerodynamic components. While the aerodynamic element is rotating, the acoustic field is not. Numerous improvements have been made in acoustic computations over time. Essential technological techniques and applications have been reviewed in several of these contributions. The workout acoustics computations employing a hybrid approach for noise transmission and far-away-area estimate are reviewed in this article.

2.2 Turbulence Flow Modeling Methods for Hydroacoustic Noise Finding from Underwater Bodies:

A lot of effort has been put into understanding flow turbulence in the engineering and academic areas since it is crucial to flow transport phenomena [44]. Nevertheless, turbulence is still not entirely understood because of its complicated structure, including instantaneous and intermittent properties. A wide-ranging variety of geographical and temporal scales, as well as substantial nonlinearity [45]. Various levels of precision can be achieved while numerically resolving turbulent flow. The RANS [46], LES [47], and the direct numerical simulation (DNS) techniques [48] are only a few of the several numerical methods that have been suggested to solve turbulence. Due to its comparatively high-level precision in forecasting the mean flow characteristics and its lower arithmetic requirements, the RANS technique, notably the Eddy Viscosity Model (EVM), is one of these numerical approaches that is frequently employed for computing turbulent flows. However, this method has several flaws, such as degraded accuracy

and uncertainties brought on by model development assumptions and inadequate integration of fluid physics. The LES and sub-grid-scale (SGS) eddy are the two categories into which the whole eddy range is divided in the LES technique. The former can be estimated using the SGS model, whereas the latter can be directly resolved. This method is widely utilized to research turbulence behavior and settle small-to-moderate Reynolds number (RN) streams as processing power improves quickly. For LES modeling, more consideration is given to inflow boundary conditions and network density to generate relevant results. The DNS methodology is the most precise numerical approach compared to the LES and RANS since it directly resolves all turbulent eddies without using models. To handle turbulent engineering flows, DNS, however, has large computational requirements that are impossible for the existing processing capacity to meet. Furthermore, the massive volume of data produced by DNS should be closely examined.

Numerous model versions to handle specific turbulent flows have been presented because of the RANS method's uncertainties [49], which makes it difficult for users of computational fluid dynamics (CFD) algorithms to choose the best model for their situations. Although there are some studies regarding turbulent flow modeling[50], a thorough and well-coordinated explanation of the model interpretation and development is highly beneficial in determining the applicability of various models. The inflow boundary condition, in addition to SGS models of the LES approach, is a crucial component of the simulation. A thorough examination and description of the procedures is required and beneficial for the LES model user, given the variety of ways to provide inflow information [51]. Clarifying the capabilities and present constraints of the DNS approach is necessary to appreciate its potential fully. Model validation is required in addition to numerical results for turbulent flows to guarantee the precision of the simulation. Different physical experiments supported by measurement methods are carried out in accordance with various research to validate the numerical model. Studies have concentrated on the principles of various measurement methods, data interpretation, and applications [52]. However, it is necessary to talk about how well physical testing and modelling translate modeling for all applications in the industry. For accurate data to be obtained, assessing the measurement methods' limits and progress is essential. This paper discusses the formulation and advancement of the three primary numerical techniques for turbulence modelling, namely the RANS, LES, and DNS.

2.2.1 RANS

The RANS equations are a collection of mathematical equivalences that illustrate the turbulence attributes of a fluid. They are obtained by averaging the RANS equations over a finite time or spatial region. The RANS equations are given by:

Continuity equation:

$$\frac{\partial(U_i)}{\partial x_i} = 0$$

Momentum equation:

$$\frac{\partial(U_i U_j)}{\partial x_j} + \frac{\partial p}{\partial x_i} = \frac{\partial \left(m_u \frac{\partial U_i}{\partial x_j} + m_u \frac{\partial U_j}{\partial x_i} \right)}{\partial x_j} + F_i$$

where U_i is the fluid velocity, p is the pressure, μ is the dynamic viscosity. The term $\partial \left(m_u \frac{\partial U_i}{\partial x_j} + m_u \frac{\partial U_j}{\partial x_i} \right)$ represents the viscous stress tensor.

Energy equation:

$$\frac{\partial(U_i T)}{\partial x_i} + \frac{\partial(U_i q)}{\partial x_i} = \frac{\partial \left(k \frac{\partial T}{\partial x_i} \right)}{\partial x_i} + Q$$

where T is the temperature, q is the heat flux, k is thermal conductivity, and Q is the heat generation rate.

2.2.2 k- ω & k- ϵ Model

The two basic equation models used in industrial engineering are the k- ϵ and k- ω turbulence models. k stands for the kinetic energy of turbulence. The symbol represents the turbulence energy dissipation ratio. The conversion of k into internal thermal energy is represented by the dissipation ratio, which is equal to k . A different method for defining turbulent scales of complex flows is contained in the k model, which was offered as an improvement to the mixing-length model. In this model, which unites CFD to reproduce and isolate average flow properties, transport equalities describe turbulence [53]. The k- ϵ (k-epsilon) model is a mathematical model used to describe turbulence in fluids. It is established on the RANS equalities and is used to predict the turbulence traits of a fluid. The k- ϵ model equations are given by: Transport equation for k :

$$\frac{\partial(U_i k)}{\partial x_i} + \frac{\partial(U_j k)}{\partial x_j} = \frac{\partial\left(\frac{\nu_t \partial k}{\partial x_j}\right)}{\partial x_j} - \frac{\partial\left(\frac{\nu_t \partial k}{\partial x_i}\right)}{\partial x_i} + P_k - D_k$$

where U_i is the fluid velocity in, ν_t is the turbulent viscosity, P_k is the creation, and D_k is the dissipation of turbulent kinetic energy, respectively

Transport equation for e :

$$equal \frac{\partial(U_i e)}{\partial x_i} + \frac{\partial(U_j e)}{\partial x_j} = \frac{\partial\left(\frac{\nu_t \partial e}{\partial x_j}\right)}{\partial x_j} - \frac{\partial\left(\frac{\nu_t \partial e}{\partial x_i}\right)}{\partial x_i} + C_1 * P_k - C_2 * \frac{e^2}{k}$$

where C_1 and C_2 are constants. The $k-\omega$ model ($k-\omega$ model) is a two-phase flow model developed by Wilcox and is widely used to forecast the performance of two-phase flow systems, such as those found in nuclear reactors, boilers, and gas pipelines.

2.2.3 Shear-Stress Transport (SST) Model

Mente initially proposed the SST turbulence model in 1994. To explain border layer flow with unfavorable pressure slopes, turbulent shear transport is included in this model. SST is a 2-equation eddy-viscosity turbulence model whose primary goal is to forecast solutions to common engineering problems. It comprises specifically of the k and k turbulence models [54]. Simple Dirichlet boundary situations are accessible with the k model since it is applied in the internal area of the boundary layer without a damping purpose. The k model is seen to be a fair deal for the free shear flow. Extensions like SAS and laminar turbulence transition may be built on top of the shear-stress transport model as a base. Karman length-level is incorporated into the turbulence level equivalence of SST-SSA (scale-adaptive simulation), which is one common example. So, it is possible to dynamically solve the turbulent spectrum of unstable situations. While switching to the average RANS model in sections of balanced flow, the SST-SSA model behaves similarly to LES behavior in unsettled zones [55].

2.2.4 Advanced Eddy Viscosity Model

The Eddy Viscosity Model (EVM) includes all the techniques above. Other cutting-edge EVMs were created [56, 57]. Durbin [58] introduced a new turbulent viscosity term that is thought to be more suitable in a near-wall area with the purpose of significant anisotropy in the nearby-wall territory. The advanced eddy viscosity model (AEVM) is a mathematical model used to

predict the turbulent flow of fluids. It is based on the hypothesis of an eddy viscosity, which represents the ability of a fluid to transfer momentum due to the existence of turbulent eddies. The AEM model is commonly used in CFD simulations to predict the behavior of turbulent flows. The model is based on the RANS equations, which describe the motion of fluids under various conditions. The AEM model modifies these equations by adding a term that exemplifies the influence of turbulent eddies on the flow.

2.2.5 RN Stress Model

Second-Moment Closure (SMC) models rejecting the Boussinesq hypothesis have been devised to get around the EVM's restrictions. Each of the RN stress terms is immediately solved by the SMC model using the transport equation. Long projected to take the role of the presently popular two-equation models, the SMC method more carefully contemplates the impacts of simplified curvature, cycle, and fast change in strain rate. The algebraic and differential stress models comprise the SMC model class (DSM). The weak-equilibrium assumption is used to construct ASM from differential stress transport equations [59]. By supposing that the transport of the RN stress is proportionate to that of turbulent kinetic energy, it overlooks the transport terms of the anisotropy [60]. Between the LEVM and the DSM, the ASM is often seen as a steppingstone instrument. The RANS model is a mathematical model used to illustrate the turbulent flow of a fluid. It is based on the RANS, a set of calculations demonstrating rated behavior. The RN stress model is used to foresee the turbulence structure of a fluid flow and is commonly used in CFD simulations. The RN stress model is built on the perception of RN averaging, which involves averaging the fluctuations of the fluid flow over a sufficient period. This allows for separating the mean flow from the turbulent oscillations, which can be described using a set of transport equalities for the RN stresses. The RN stress transport equations are given by:

$$U'_{ij} = -\left(\frac{1}{\rho}\right) * \left(\frac{dU_i}{dx_j} + \frac{dU_j}{dx_i}\right) + \left(\frac{2}{3}\right) * k * \delta_{ij}$$

where U'_{ij} is the RN stress tensor, U_i is the velocity component, ρ is the fluid density, k is the turbulent kinetic energy, and δ_{ij} is the Kronecker delta function.

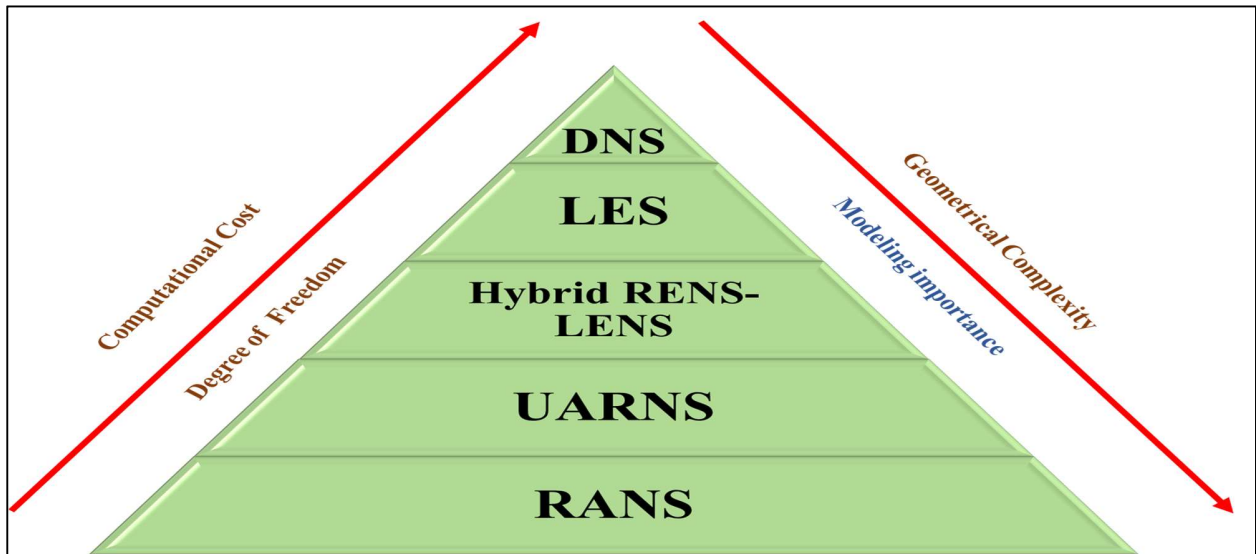


Figure 2.1: Turbulence models Comparison for Hydroacoustic Noise Finding

2.2.6 LES

Eddy scales in turbulent flow range widely, from the Kolmogorov length scale to sizes that are analogous to the mean flow's typical characteristic length. The advantage of turbulent energy is included in the huge eddies, which also provide most of the momentum and transmission of energy. Boundary states have a considerable influence on them. The dissipation of minor eddies is influenced by the fluid's viscosity and is more isotropic and homogeneous. Because they are, modelling all the eddies in a single RANS model is immensely challenging using a realistic filtering approach [61] for the instant controlling equations; the LES methodology isolates the major eddies from the small ones. Then, the filtered equation directly resolves the large eddies, while the SGS model models the little eddies, also known as SGS eddies. An SGS model is a mathematical model used to represent the effects of small-scale phenomena on fluid flow behavior. These phenomena often referred to as "sub grid scales," are too small to be resolved by the numerical grid used in CFD simulations. One common SGS standard is the Smagorinsky model constructed on eddy viscosity. The eddy viscosity characterizes the impact of the unsolved turbulent variations on the mean flow. The Smagorinsky model is given by:

$$\nu_t = C_s^2 * \text{total Delta}^2 * |S|$$

where ν_t is the eddy viscosity, C_s is a model coefficient, Delta is the grid dimension, and S is the straining rate tensor.

2.2.7 DNS

The DNS model, with no use of a turbulence model, numerically resolves the 3-dimensional, time-dependent NS equations. The DNS approach employs a tiny mesh and a small-time step to capture all the turbulence scales in the supplied flow. The extraordinarily high computational resource needed prevents the DNS technique from being applied. The quantity of grid points is considered proportional to $Re^{9/4}$ in a DNS case. Since the eddy size in the near-wall region is lesser than that in the exterior domain, a more refined mesh is essential to fully settle the turbulence in the near-wall region, thus increasing the grid points. The DNS technique is currently not feasible for most practical flows because of the vast computational domain, complex geometry, and high RN number in practical engineering. On the other hand, a surprisingly high computing performance for DNS has been attained thanks to the ongoing parallel computing approach development [62], hybrid CPU + GPU computing architecture [63], and sophisticated numerical algorithm [64]. High-performance computing is currently facing new difficulties. Due to space constraints, this topic is not discussed in this work; nevertheless, readers can be engaged with relevant results for more evidence [65]. The DNS (Direct Numerical Simulation) model exists as a computational method used to study the behavior of fluids at high RN numbers, which is a ratio of inertial forces to gelatinous forces in a fluid. In the DNS model, the RANS equations, which illustrate the motion of fluids, are solved numerically without simplifying assumptions or modeling. The RANS equations are a set of partial variance equations describing a viscous IF's action. The DNS model is mathematically sophisticated and calls for substantial computational resources, but it enables highly accurate simulation of complex flow phenomena. To study turbulent flow, it is frequently used in conjunction with other modelling techniques, such as LES. The performance comparison of various turbulence models is shown in Figure 1.

2.2.8 DES

After changing the SA turbulence model's dissipative component, Scalar introduced the DES model in 1997 [66]. The increase in dissipation tries to decrease eddy viscosity in the area distant from the wall. The DES model functions as the earliest SA model in the wall region. This stops the model from anticipating "premature" division and prevents moving from RANS to LES too near the wall. The DES model comprises the RANS and LES turbulence models, where the RANS model operates in boundary layers and switches to the LES model for more extensive,

disconnected flow areas [67, 68]. Reference [69] provides a detailed summary of the relationship between the DES, RANS, and the LES model. The DES model relies on flow variability to enable rapid production. The simulating scenario built on the DES model should be thoroughly modelled to account for the influence from direct mesh to the RANS model. Additionally, the DES model supports RANS and LES mesh transformation. The comparison among numerous turbulence models in the context of advantages and disadvantages is given in Table 1 as follows.

Table 2.1: Evaluation of Numerous Turbulence Models in Context of Benefits and Shortcomings [70]

Model	Advantages	Shortcomings
SA	No wall function, and strong convergence	Unsuitable for separation flow and shear flow problems.
$k - \epsilon$	Suitable for long-distance, non-separated turbulent flow	Insensitive to flow with separated boundary layers and inverse pressure gradients. It is challenging to compute.
$k - \omega$	Suitable for internal, curvature, jet, and separated flow, etc.	Compared to k , convergence is more challenging, as outcomes depend on the beginning circumstances.
SST $k - \omega$	In the internal area of the boundary layer, where there is no damping function, usage of the $k - \omega$ model changes to the $k - \epsilon$ model for the free shear flow.	SST models show reduced sensitivity to free stream conditions compared to the previous two-equation turbulence models.
LES	Using sub grid scale to simulate minor eddies while geometric computation is necessary for big eddies	It requires a precise grid and tiny time increments to calculate the near-wall area.
DES	Appropriate for peripheral aeroacoustics wall turbulence, aerodynamic, and other phenomena	Due to the change from RANS to LES, mesh creation is more challenging.

Transition	Useful for resolving the turbulentization of laminar flows	Boundary circumstances bring on calculation challenges.
Multiphase	Determining the connection between flow patterns and mechanical structure defining the various fluid phases	The inaccurate mathematical description of multiphase flow makes the momentum transfer across multiple phases complicated to predict.
Cavitation	To explain how the liquid and vapor phases change one another	Unreliable cavitation mathematical definition

2.3 Using Acoustic Analogies and Turbulence Models for CFD in Cylindrical Bodies Considering Different Factors

In the discipline of aeroacoustics, much time is spent looking into the noise made by flow past cylinders. For instance, the turbulent three-dimensional flow across sharp-cornered rectangular cylinders with aspect ratios ranging from 0.40-4.0 has been studied in [71]. According to the data, the Strouhal headcount has been falling with an expansion in the side ratio (from 0.40 to 2.50), with the highest drag coefficient amounts occurring at a side ratio of 0.62. By taking into account both the Curli's interpretation and a description created on the Green's function, the flow-stimulated of a circular cylinder noise has been explored [72]. By solving IF RANS equations, it is possible to determine the flow field around the cylinder. For small Mach values, the findings showed that the dipole-field predominated over the quadrupole-field. When choosing the amount of noise in the stream around a circular cylinder in the crucial zone, a compressible LES in conjunction with the FWH equation on solid and porous surfaces has been employed [73]. The dipolar tone emitted by a vortex was found to be the main source in the far field. At low frequencies, wake oscillations and at high frequencies, Kelvin-Helmholtz (KH) instability were shown to be two additional broadband noise sources. The authors in [74] have conducted an investigational exploration of the emanated noise of square finite-length cylinders over a different assortment of aspect ratios. At small aspect ratios, the wake was dominated by spanwise flow, which led to an extension of the vortex growth length and a considerable decrease in the flow noise at an aspect ratio of 7.5. Larger aspect ratios' primary noise generators were filaments of inclined vortices. The vibrant noise attributes of square and circular limited-measurement cylinders were studied experimentally by Moreau and Doolan [75] in a wind tunnel at different flow speeds and

for different aspect ratios. The findings showed that the emitted sound field exhibited emission characteristics like those of a dipole. One dominant acoustic tone was heard for cylinders with aspect ratios between 9.7-17.8 and 1.9-7.8 for circular and square cylinders, respectively. But two dominant styles were produced for cylinders with aspect ratios above 8.7 and 19.4 for square and circular cylinders, respectively. Wang et al. [76] analyzed the far-field noise and the impact of the aspect ratio on the flow through square cylinders. The nearby-field flow characteristics were obtained using DES, and the far away-field noise was forecasted using the FWH equation for RN numbers between $5e4$ and $2e5$. As the aspect ratio was raised, the maximum sound pressure level rose in magnitude, albeit the location of the significant peak frequency remained the same.

However, research on the hydro-acoustical noise processes of square, rectangular, and circular cylinders still need to be completed. An experiment to study the flow field around rectangular cylinders in a water tunnel at RN numbers among $2e4$ and $7e4$ was conducted in [77]. The drag factor rose with a rising side ratio, reaching a limit at a side ratio of 0.62 before declining. Numerical analysis was performed by Choi et al. [78] to determine the impact of quadrupole generators on the background noise across a circular cylinder. A comparison was made between the FWH equation with and without the quadrupole noise source in a permeability preserving FWH equation. Although the two approaches differed by an average of 5 dB across the board, they tended to provide the same results in terms of general frequency characteristics. A simplified version of Brentner's quadrupole formulation was employed by Choi et al. [46]. Same formulation was compared to experimental data and the permeability FWH equation, all while considering quadrupole sources. Specifically, regarding the highest possible sound pressure level, achieved formulation was more reliable than the permeable FWH. A numerical investigation of the hydro-acoustics of a sphere and a cube immersed in a uniform water flow was explored in [12].

The acoustic investigations employed a mixture approach, merging FWH acoustic analogy and LES. It was found that the wakes created by a sphere and a cube were more powerful than those made by a prolate-sphere. In the case of the sphere and cube, the nonlinear components contributed more to the total noise than the linear ones did, but the situation was reversed in the case of the prolate sphere. Cianferra et al. [79] examined the performance of the Curle, direct, porous, and full porous formulations for solving the FWH problem. These formulas foretell the amount of noise produced by a finite-dimension submerged square cylinder. They compared the

benefits and limitations of various solution methods, suggesting a hybrid method that combines the improvements of the spongy interpretation with the assessment of capacity critical conditions. Analyses of the hydroacoustic and aeroacoustics systems' findings. Applying the FWH equation for hydro and aero acoustic issues allowed for three and two-dimensional flow noise estimates for a circular cylinder [80]. It was found that 3-dimensional imitations were effective in forecasting in cooperation with the highest sound pressure limits and the wide band noise stages; however, 2-dimensional models needed to be revised to approximate the broadband noise levels. DES-FWH and RANS-FWH hybrid techniques examined how temperature and salinity ratio affected a circular cylinder's hydro- and aeroacoustics properties [81]. It was discovered that the sound pressure stages for the water and air media increased in response to temperature increases, respectively. The central peak frequency remained almost constant. However, the sound pressure limits improved as the salinity ratio rose. The main peak frequency also changed with the temperature of the air but not the temperature of the water, increasing with the former. In a separate investigation, the effectiveness of the LES, RANS, and DES techniques for predicting the hydroacoustic properties of a submerged cylinder was explored [82]. The mixture approach, LES-FWH, produced findings most closely related to the experimental data. While the hybrid approaches RANS-FWH, DES-FWH, and acoustic measurements showed acceptable agreement, RANS (k-Realizable)-FWH exhibited low understanding. The findings showed that the combination technique RANS (k-SST)-FWH was a suitable approach for conducting acoustical analysis due to its excellent performance and cheap computing cost. The effects of symmetrical factors on the hydrodynamic and hydroacoustic fields of submerged bodies were studied by Bulut and Ergin [83]. It was discovered that geometric factors significantly affect the bodies' hydrodynamic fields and produce un-favorable noise levels. The fluid velocity and aspect ratio rose, but the cylinder diameter decreased, and the sound pressure levels did not.

Circular cylinders are the only kind of object studied before. The few published investigations on the flow noise processes of rectangular, circular, and square cylinders are limited to aeroacoustics issues. This study is a thorough investigation that builds on the authors' earlier work by presenting new numerical and experimental facts on the hydro-acoustic properties of cylindrical bodies with various aspect ratios, diameters, and side ratios, respectively, circular, rectangular, and square cross sections. To significantly contribute to the result of multiple hydroacoustic issues, a systematic investigation is conducted to get a more profound knowledge

of the intricate underwater noise processes. Dynamic and acoustic simulations were accomplished using the multi physics CFD software STAR-CCM+ [84]. Circular cylinders measuring 65.0 mm and 19.0 mm in diameter were subjected to experimental hydroacoustic dimensions. Comparing the outcomes of the hybrid method and experiments was done as part of the validation study. Circular cylinders with different aspect ratios and diameters were used to determine the hydro-acoustic properties. The impacts of side proportion on the hydro-acoustic attributes were analyzed for cylinders with rectangular and square cross segments. The wet area is identical to the cylinders used in this section. It has been found that the investigational measurements and the arithmetical calculations agree very well.

Different research papers were analyzed and are discussed in detail in this section having similarities with this research. Three bodies were analyzed: a cube, a prolate spheroid, and a simple sphere. Modeling turbulent flow is done with LES, while FWH is used as a sound analogy. Both models were created in an Open-FOAM environment using the finite volume method. Grid data for different [110] provides the geometry to obtain the analysis. The simulations were validated using two unstructured body grids, coarse grid (CG) and fine grid (FG), comprising 5 million and 8 million cells, respectively. Two grid outcomes have been compared with DNS data and experimental data. RN's number is the same for comparison in different cases. In the results, CG gives products comparable with DNS. However, FG has a better velocity profile. This may be due to a change in the structure of both analyses. The skin friction coefficient gives efficient results as compared to the DNS. The pressure coefficient has been compared with experimental data [111]. LES gives better results for both scenarios. Use at the minimum angular direction of 71 degrees. Overall, FG produces better outcomes than CG. Also, for bluff bodies (cubes and spheres), the contribution of FWH linear terms to the noise signal is more significant than that of non-linear terms. But for the prolate spheroid, nonlinear terms make up a more substantial part of the noise signal because their shape makes the loading noise almost disappear. Also, the comparison shows that aspect ratio impacts linear and nonlinear terms. Furthermore, three-dimensional and dimensional objects influence the generation of hydroacoustic noise [12].

A hybrid method that cartels RANS and FWH has been employed for the circular cylinder with several aspect ratios and diameters. As the diameter of a circular cylinder goes up, the overall and the highest noise pressure level go down. At the same RN number, as the diameter

of the circular cylinder gets more petite, the wake area gets more chaotic. As the thickness of the circular cylinder grows, the vortex development moves downriver. The broadband noise level, the overall, and the highest sound force also improved with a rise in aspect ratio. The wetted surface section of the cylinder also increases with a growth in aspect ratios. This paper also looked at how the speed of the fluid affected the hydroacoustic properties. The side ratio also indicates the different impacts on the hydro-acoustic characteristics of different cylinders [79]. The acoustic attributes of the circular cylinder are attained by contemplating the effects of fluid type, temperature, and saltiness ratio. Other parameters, such as the mean central frequency, broadband noise, overall sound pressure, and sound pressure level, were used to measure these effects. An increase in temperature difference decreases water density and viscosity. But when the air temperature increases, the viscosity increases, and the density decreases. The central peak frequency shows no impact on water salinity. However, the broadband noise declines with a rise in water temperature but improves with a growth in air temperature [81].

One of the paper reveals novel findings about the hydro-acoustic investigation of the BB2 submarine [112]. The flow field calculation and the acoustic assessment are suitable for the methods provided herein. Wall-modeled LES enables the computation of turbulence at a cheap cost while maintaining adequate accuracy, particularly for the wake. The FWH-based acoustic relation, presented here in an advective way for both linear and nonlinear variables, enables the calculation of the acoustical field using the fluid-dynamic data after processing. The ability to extract the detailed-range noise of the underwater beginning from the model-level simulation is made possible by the exact resemblance between the sound quality of the submarine at model dimension and full size. The float and its extremities in the near area influence the bigger partial-wake plane. At the same time, the other line of work, creates by the equilibrium resemblance theory for an axial-balanced form, according to an analysis of the hydrodynamic field. The information needed to fully understand the acoustic field has been processed using the findings. Non-linear noise sources dominate the flat ($z = 0$) and diagonal ($y = 0$) directivities, producing a pattern like a canonical quadrupole that is warped in the wake's direction. By appropriately alimentation the kernel of the integrals making up the non-straight analog of the FWH comparison, it has been shown that a qualitative-wise equivalent directiveness shape may be achieved. All the characteristics required to depict a schematic of the directivity are present in a simple structure of 2 sources with a velocity like that which may be seen near the hull. The

examination of the acoustic pressure limit reveals broad-banded bands instead, yet they exhibit distinctive peaks in some occurrences. These spectra and particular flow events, notably the enormous separations at the stern, might be connected according to coherence analysis. The high-frequency noise propagates away from the submarine because of the eddies' dissipation. In the current study, several numerical approaches to the FWH equation have been evaluated, and the sound produced by a physique submerged in a constant flow was explored [79]. To account for the non-linear influence of the noise-generating process, the convective form of the quadrupole term was devised. In this analysis, Curle, the typical porous, and the direct method have been analyzed where nonlinear components are immediately considered while calculating the integral volume terms. Only with close sources, and therefore when time delays are not significant, is it possible to account for volume integrals. The notion of a compact noise source often appears in literature. A thorough explanation is put out in the current study, based on a dimensional analysis that considers the maximum frequency, source length, and good quickness. It provides criteria created on the value of the non-dimensional constraint MFP. The direct volume assimilation and the FWH porous interpretation are used in an acoustical monopole field to verify the time delay analysis. To evaluate the functioning of the immediate integration with that of the porous approach, the basic instance of an irrotational vortex has been applied, demonstrating that the direct integration does not deteriorate from the end cap concern, which is common with the porous method. A fluid dynamics issue in the incompressible domain has been considered while evaluating the approaches. At $Re = 4000$, the stream around a fixed-size cylinder with a square unit was examined. Despite being straightforward, this scenario illustrates several interesting facts about the creation and spread of vibrant fluid noise. It is distinctive for two reasons: first, it has a chaotic wake and a whirlpool sheet, which results in considerable involvement from the FWH quadra pole source terms; and second, it is a typical example of a broad class of engineering challenges. Wall-resolving LES was used to solve the fluid-dynamic field, and the results were confirmed using data from the literature. To guarantee the correctness of the findings, we used the multi-step fractional action PISO method, which is accurate to the second order in both space and time and had a Courant figure that was far lower than the stability limit. As a result of the little part that compressibility delays play, this simulation offers the data that the acoustic solvers need as input and a reference pressure that can be used to evaluate the accuracy of noise predictions. It has been shown in previous research that the stream field that

LES produces is correct for auditory purposes. This is since the unsettled scales do not impact the noise that is transmitted. The noise caused by fluid dynamic stresses acting on the body's surface is only significant in an adjacent space close to the body. Besides this, the Curle solution is insufficient to assess the noise mark in the vicinity of a vortices ground, such as the one forming towards behind the cylinder. The porous interpretation accurately foresees the whole pressure continuum, albeit the outcomes depend on the location of the size sites, the integration domain used, and the grid solution. On the other hand, the direct method produces a sound forecast in accordance with source data at sites where (corresponding to the basic hypothesis on which the FWH equation is established) the pressure is described by minor agitations. This technique can be easily put into practice, gets the most out of the fundamental CFD solution, and creates further resilient computations in the face of variations in the radiating domain. However, its usefulness now is restricted to issues in which the impacts of fluid-dynamic squeezability on noise spread may be ignored (little Mach number). As a powerful technique for solving the problem, we suggest the completely porous, which refers to the initial formulation and considers the influence of the quantity outside of the permeable face. In this assessment, the surface under consideration has a pyramidic form. In this regard, it is possible to see the full porous as an alternative to the porous formulation where the end-cap issue is resolved. The entire porous technique is better compared to the acoustic solution to the conventional porous formulation.

A study investigates using FWH to estimate the flow noise around a cylinder in both 2 and 3 dimensions [83]. Again, the flow field data were acquired using CFD for the acoustical studying of the realizable two-layer k-e turbulence model with SST k-w; the turbulent is simulated. Each turbulent model's capacity to anticipate has been investigated during the research. Auditory investigations include the evaluation of the monopole, dipole, and quadrupole acoustic signals. Comparisons are made between the measured sound pressure levels for a circular cylinder and extensive experimental findings published in the literature. Additionally discussed and recommendations are correlations of the flow noise estimates made in 2 and 3 dimensions for the vicinity of a cylinder.

Table 2.2: Drag coefficient and Strouhal number Comparisons for Circular Cylinders with Change in Dimensions in Medium of Air and Water

Medium Water				Medium Air			
Model	Drag Coefficient	Model	Strouhal number	Model	Drag Coefficient	Model	Strouhal number
Experimental [113]	1-1.4	Experimental [114]	0.19	Experimental [115]	0.98	LES (3-D) [116]	0.20
k- ϵ (2-D) [117]	0.48	Experimental [118]	0.20	LES (3-D) [119]	1.01	LES (3-D) [120]	0.21
LES (3-D) [117]	1.08	k- ω (2-D) [117]	0.25	LES (3-D) [121]	0.97	LES (3-D) [121]	0.21
k- ω (2-D) [117]	0.94	k- ϵ (2-D) [117]	0.28	LES (3-D) [120]	0.97	LES (3-D) [119]	0.22
k- ω (2-D) [83]	0.84	k- ω (2-D) [83]	0.25	k- ω (2-D) [83]	0.72	k- ω (2-D) [83]	0.29
k- ϵ (2-D) [83]	0.49	k- ϵ (2-D) [83]	0.29	k- ϵ (2-D) [83]	0.51	k- ϵ (2-D) [83]	0.28
k- ω (3-D) [83]	1.19	k- ω (3-D) [83]	0.23	k- ω (3-D) [83]	1.12	k- ω (3-D) [83]	0.24
k- ϵ (3-D) [83]	0.99	k- ϵ (3-D) [83]	0.28	k- ϵ (3-D) [83]	1.17	k- ϵ (3-D) [83]	0.24

In this research, a numerical approach is provided to investigate the impact of the marine automobile flow field on the operational performance of the towed sonar cable array positioned on the top propeller [122].

2.4 Computational Fluid Dynamics (CFD) Simulations

CFD reduces the number of experiments, time for designing, and cost. Several software programs are used for simulations of turbulence flow, which has been discussed in this section. In [85], the influence of the direction of inclination on fluid movement in a pipe was explored using numerical simulation. This was done by taking into consideration several different viscous models.

Using the k- turbulence model in ANSYS FLUENT, an internal flow study review of a dump diffuser is a component found in naval gas turbines and modern aviation engines. They came to the conclusion that increasing the diffuser angle would have no influence on the diffuser's effectiveness [86]. The stable IF seen using the CFD approach across a T-junction may be found in [87]. They established the investigational framework to get the reference data produced when fluid travels through the T-junction of the pipe. They also employed the exact data for the CFD study that was conducted with the assistance of FLUENT and ANSYS. Spooner et al. fabricated various compositions with trifurcations and bifurcations that result in head shortfalls in a fluid structure [88]. They also provided quantitative data of sharp-edged bifurcation loss coefficients that CFD derived. Gedik et al. conducted an investigational and computational analysis of the stream of magnetorheological fluids in circular pipes when a uniform magnetic field was present using CFD [89]. The use of the CFD approach was put to use in order to study the influence that various components have on the pressure that is created on the pipe wall in [90]. Using CFD analysis, the effect of the velocity of turbulent fluid movement and mass drift rate and along the length of pipe in a trifurcation pipe branch under different RN's number of fluid in a pipe was examined [91], and they also utilized the CFD software COMSOL for the determination of NS IF. The flow properties of different immiscible liquids, were observed by applying ANSYS-FLUENT in [92]. To determine the most effective meshes for laminar and turbulent flow, the influence of mesh autonomy in a 3-dimensional pressured fluid flow for velocity profiles was examined in [93]. A laminar single-phase water flow using CFD at different RN numbers in a hollow helical pipe was analyzed in [94]. ANSYS was applied to analyze flow through a pipe at discrete points and calculate losses in the head caused by modifications to the pipe's design [95]. Through CFD research, it has been observed that the resistance coefficient fluctuates with changes in flow parameters [96]. In order to learn more about where one flow pattern ends, and another begins, CFD simulations were performed in [97]. ANSYS-CFX was applied to study the bend/turn effect for a Y-shaped pipe [98]. The SST model was used in ANSYS-CFX to examine the flow disciplines of a Y-junction and a T-junction pipes [99].

Scale resolving simulation and RANS/URANS transition turbulence approaches have been compared using commercial ANSYS programs. Studies have shown that most turbo machinery design analysis is computationally feasible and appropriate for CFD [100]. Due to the complexity of this physical show, flow field models for forecasting the impact of turbines performing on free

surface flow scenarios have also been utilized [101]. In addition to ANSYS, STAR-CCM+ has also been used for CFD applications, as examined in the literature [102]. For instance, Airflows in passenger vehicles, aero plane cabins, and structures have all been modelled using STAR-CCM+. ANSYS has, however, been used for buildings, ships, and aero plane cabins. Due to the high cost of licensing, designers prefer to work with a single vendor even though both programs have been used effectively to model interior airflows [103, 104]. Previous studies used ANSYS Fluent and STAR-CCM+ to forecast indoor air distributions. The two plans for air distribution in an ambulance waiting room were contrasted in [105]. They concluded that because ANSYS Fluent can obtain the precise point value of any variable at any place, it was a suitable tool for modeling a complicated interior environment. However, only certain sites can get a variable's value via STAR-CCM+. The achievable k-model in ANSYS-Fluent was compared to the RN stress model in STAR-CCM+ for heat and mass transfer in a ventilated environment [106, 107]. It was suggested that the RN stress model in STAR-CCM+ be used instead of the k- model since it predicts the temperature and velocity distributions better. However, these comparisons could not assure consistency due to the inclusion of several variables in various cases. Furthermore, more than 90 solvers are presently included in Open-FOAM, including DNS, heat transfer, combustion, compressible and IFs, stress analysis of materials, electromagnetics, finance, etc. Compared to CFD toolkits offered commercially, Open-FOAM offers distinct benefits. To solve an issue, the codes may be changed. Additionally, by changing the current solvers, new solvers can be produced. As a result, several CFD analyses have been conducted and are available using the Open-FOAM program [108, 109].

CHAPTER 3: METHODOLOGY

The most recent version of the STARCCM+ is used to import different CAD models for computational fluid dynamics (CFD), which is mostly used for simulations. CFD uses several techniques to numerically solve the pressure and velocity fields inside the control volume in order to model the flow. The process of CFD simulations consists of three major steps:

- a) Pre-processing (Element types for Mesh Generation, physics models)
- b) Solver (Convergence study, Mathematical equations)
- c) Post Processing (Graphs, Plots, Data collection)

Performing CFD requires setting up initial boundary conditions. These conditions are processed with different environmental factors and outcomes of computed calculations are analysed for determining various effects related to fluid dynamics. The complete process was carried out using STAR CCM+. There are other software's for performing similar tasks but they lack ingenuity and user-friendliness. Graphical User Interface (GUI) provided by the Siemens developed software is another major advantage of choosing this software and it has dedicated marine analysis tool for further evaluation and post processing.

The next section provides detailed workflow of the three major steps discussed earlier. Star CCM+ is a standard commercial software package designed and owned by Siemens Corporation ltd. Software used for Finite Volume approach to solve CFD problems. Selection of this software was due to high number of research articles in marine industry as well as software offers a huge number of problem-solving capabilities of naval and marine related problems.

3.1 Pre-Processing

Pre-processing involves the setup to be made before starting the simulation. These setups are being discussed in coming article.

3.1.1 Grid Generation

There are two types of grids being used in STAR CCM+ in discretizing the fluid domain

- Structured Grid (Trim Cell, Extruder, Prism Layer Cell)
- Unstructured Grid (Polyhedral, tetrahedral)

It is however important to note that some meshes are being used solely for the surface discretization while some are utilized for volume discretization. Also one may inquire the importance of choosing grid type so following are some of the characteristics of choosing mesh type

- Choosing Mesh type highly depend on convergence
- Appropriate mesh would reduce the computational time significantly
- How accurate solution is depending on grid type as well

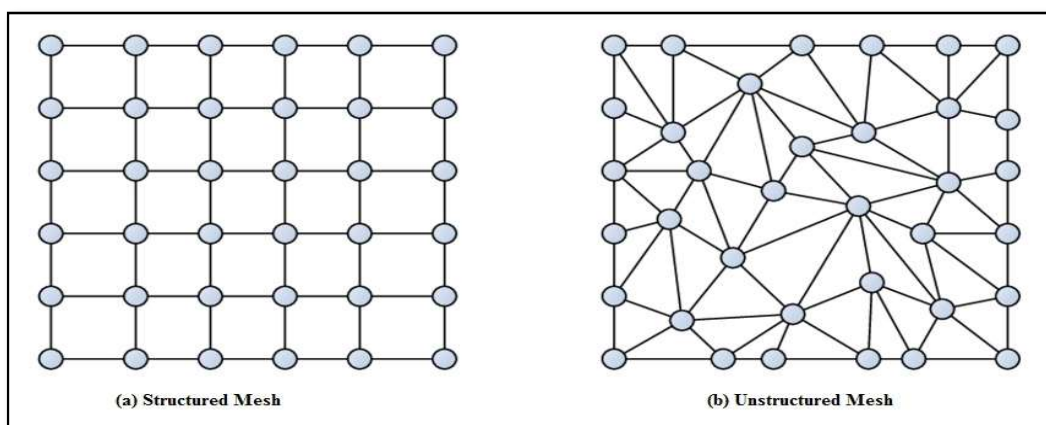


Figure 3.1: Grid generation (structured and unstructured mesh)

3.1.1.1 Structured Grid

Structured grids are used for the flows where complexity and turbulence of fluid particles is known by the user. In that way user can have freedom to select the mesh density in whatever way it should comfort. Smooth grid framework may be achieved just like rectangular matrix array. They are simple to execute as well as productivity is high.

3.1.1.2 Unstructured grid

Unstructured grids are usually very beneficial where the meshing of the part which should have complexity in geometry. Unstructured grids are universal because it is applicable for all geometries. All nodes do not equally distribute around the domain. So, the structure of data is not in regular shape as shown in figure 3.6.

3.1.1.3 Trimmer Mesh

Trim cell mesh is hexahedral mesh. Trimmer is mesh offered by Star CCM+ which is computationally very efficient as well as productivity is high. On the contrary to other types of volume meshes i.e. Polyhedral and Tetrahedral does not vary results if model is complex and quality of details is not dependent.

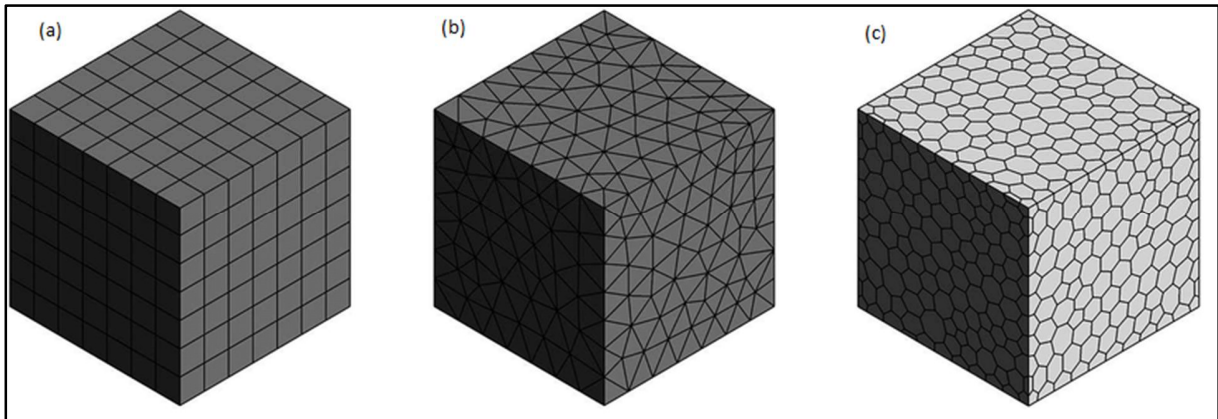


Figure 3.2: Mesh types a) Hexahedral Mesh b) Tetrahedral Mesh c) Polyhedral Mesh

3.1.2 Prism Layer Mesher

An inflated layer mesher is another name for a prism layer mesher. Prism Layer meshers are a kind of mesher that star CCM+ provides for capturing boundary layers. These meshers are used as a foundation for building layers of prismatic components in the vicinity of walls. Using the advantages of standard structured grid techniques is made possible by the prisms' (wedges') structured nature in the normal to surface direction. Prismatic grids are very good in orthogonality and grouping. The algebraic marching method is very efficient and fast. Prism Layer meshers are essential for simulations in which flow characteristics and resistance play a major role in how body parts move. These stacks of layers with comparable sizes and shapes result in a very functional and adaptable layer of cells that can quickly resolve boundary layer problems.

3.1.3 Extruder Mesher

Extruder as by name suggest is a mesh types in which mesh size is extruded in any direction specified by the user through boundary conditions selection, using extruder reduces cell count significantly

3.2 Mathematical Modeling

In this CFD approach Finite Volume approach is used as discussed above. Whereas to Reynolds Average Navier Stokes (RANS) equation is used to find the pressure and other fluid properties.

Equation of continuity and RANS is shown below

$$\frac{\partial \rho}{\partial t} + \frac{\partial(\rho u)}{\partial x} + \frac{\partial(\rho v)}{\partial y} + \frac{\partial(\rho w)}{\partial z} = 0 \quad (3.1)$$

$$\frac{\partial(\rho u)}{\partial t} + u \frac{\partial(\rho u)}{\partial x} + v \frac{\partial(\rho u)}{\partial y} + w \frac{\partial(\rho u)}{\partial z} = \mu \left[\frac{\delta^2 u}{\delta x^2} + \frac{\delta^2 u}{\delta y^2} + \frac{\delta^2 u}{\delta z^2} \right] - \frac{\partial p}{\partial x} \quad (3.2)$$

$$\frac{\partial(\rho v)}{\partial t} + u \frac{\partial(\rho v)}{\partial x} + v \frac{\partial(\rho v)}{\partial y} + w \frac{\partial(\rho v)}{\partial z} = \mu \left[\frac{\delta^2 v}{\delta x^2} + \frac{\delta^2 v}{\delta y^2} + \frac{\delta^2 v}{\delta z^2} \right] - \frac{\partial p}{\partial y} \quad (3.3)$$

$$\frac{\partial(\rho w)}{\partial t} + u \frac{\partial(\rho w)}{\partial x} + v \frac{\partial(\rho w)}{\partial y} + w \frac{\partial(\rho w)}{\partial z} = \mu \left[\frac{\delta^2 w}{\delta x^2} + \frac{\delta^2 w}{\delta y^2} + \frac{\delta^2 w}{\delta z^2} \right] - \frac{\partial p}{\partial z} - \rho g \quad (3.4)$$

In above equations μ is dynamics viscosity of fluid whereas u, v, w are the velocity component in the respective direction of coordinate axis x, y and z however g is gravitational acceleration.

The mathematical equations of the unsteady RN-Averaged Navier–Stokes (URANS) combined with the $k-\omega$ SST (Shear Stress Transport) turbulence model involve a set of conservation equations and transport equations for the flow variables and the turbulence quantities. Some of the critical equations in this model include the following:

Continuity equation: This equation describes the conservation of mass in the flow field. It is written as:

$$\frac{\partial \rho}{\partial t} + \nabla \cdot (\rho U) = 0$$

where ρ is the fluid density, U is the velocity vector, and t is time.

Momentum equation: This equation describes the balance of forces acting on the fluid in the flow field. It is written as:

$$\frac{\partial(\rho U)}{\partial t} + \nabla \cdot (\rho U U) = -\nabla p + \nabla \cdot (\mu \nabla U) + g$$

where p is the pressure, g is the acceleration due to gravity, and μ is the dynamic viscosity.

Transport equations for ω and k : These equations describe the evolution of the turbulent kinetic energy (k) and the specific dissipation rate (ω) in the flow field. They are written as:

k transport equation and ω transport equation:

$$\frac{\partial(\rho k)}{\partial t} + \nabla \cdot (\rho k U) = \nabla \cdot (\mu_t \nabla k) - \omega P_k + G_k$$

$$\frac{\partial(\rho \omega)}{\partial t} + \nabla \cdot (\rho \omega U) = \nabla \cdot (\mu_t \nabla \omega) - \omega \omega + G_w$$

Where μ_t is the turbulent viscosity, G_k is the generation of k , P_k is the creation of k , and G_w is the generation of ω . Closure equations provide a means of closing the system of equivalences, as they allow the model to predict the values of the unknown terms in the transport equations for ω and k . The closure equations for the k - ω SST model are typically written in the form:

$$\mu_t = \frac{k^2}{\omega}$$

$$P_k = -\left(\frac{k}{\omega}\right) \left(\frac{\partial U}{\partial x}\right)^2$$

$$G_k = \frac{2(\omega^2)}{k + \epsilon}$$

$$G_w = \left(\frac{1}{\omega}\right) \left(\omega^2 - C_\mu \left(\frac{\partial U}{\partial x}\right)^2\right)$$

where ϵ is a small constant and C_μ is a model constant.

The mathematical modeling of FWH's work on the flow of sound in fluids and gases is grounded on the equations of fluid dynamics and the wave equation, which defines the circulation of sound waves in a medium. These equations are combined to form the FWH equation, which

describes the interaction between sound waves and a moving fluid. The FWH equation considers various physical phenomena, such as the pressure, velocity, and density of the liquid, as well as the characteristics of the sound waves, including their frequency and wavelength. It can be used to predict the performance of sound waves in different fluid environments and to design noise control systems for various applications. The FWH equation is a valuable tool for understanding the acoustics of diverse backgrounds and for creating strategies to control noise in multiple applications, including studying aircraft noise, the noise generated by wind turbines, and the sound produced by underwater vehicles. It has also been used to understand the acoustics of concert halls and other enclosed spaces. The FWH equation is given by:

$$F^a = -p * U^a - (p + \rho * c^2) * U_j * \text{grad}^j U^a + \rho * c^2 * g^a + \lambda * (U^a - c^2 * \text{grad}^a \phi)$$

where F^a is the acoustic flux vector, p is the fluid pressure, U^a is the fluid velocity of fluid, ρ is the fluid density, c is the sound speed in the fluid, g^a is the acceleration due to gravity, λ is the mass flow rate of the fluid, and ϕ is the velocity potential. $\text{grad}^j U^a$ characterizes gradient of the fluid velocity with respect to the spatial coordinate. The FWH equation is used to predict the behavior of sound waves in diverse fluid environments and to design noise control systems for various applications. It has been extensively applied in analyzing aircraft noise, the noise generated by wind turbines, and the sound produced by underwater vehicles. It has also been used to understand the acoustics of concert halls and other enclosed spaces. The source term S^a in the FWH equation for a monopole source can be written as:

$$S^a = 4 * \pi * \rho * c^3 * q^a$$

where q^a is the source strength vector representing the strength of the monopole source. The FWH equation for a monopole source can be applied to envisage the behavior of sound waves radiated by a monopole source in a fluid environment and to design noise control systems for various applications. The source term S^a in the FWH equation for a dipole source can be written as:

$$S^a = 4 * \pi * \rho * c^3 * q^a * \left(1 - \frac{(k_x^2 + k_y^2 + k_z^2)}{(k_0^2 + k_y^2 + k_z^2)} \right)$$

where q^a is the source strength vector representing the strength of the dipole source, k_x , k_y , and k_z are the wave vectors in the x, y, and z directions, and k_0 is the wave vector in the direction of the dipole source. The FWH equation for a dipole source can be used to predict the behavior of

sound waves radiated by a dipole source in a fluid environment and to design noise control systems for various applications. In the case of a quadrupole source, the FWH equation can be written as:

$$S^a = 4 * \pi * \rho * c^3 * q^a * \left(1 - 3 * \frac{(k_x^2 + k_y^2)}{(k_0^2 + k_y^2 + k_z^2)} \right)$$

where q^a is the source strength vector representing the strength of the quadrupole source, k_x , k_y , and k_z are the wave vectors in the x, y, and z directions, and k_0 is the wave vector in the direction of the quadrupole source. The FWH equation for a quadrupole source can be used to foresee the behavior of acoustic waves emitted by a quadrupole source in a fluid environment and to design noise control systems for various applications.

Multiple approaches have been used for determining the coefficients of fundamental hydrodynamic parameters. The three essential variables and their coefficients must be calculated for longitudinal hydrodynamic control to evaluate the control performance of the cylindrical shaped underwater body. These parameters are drag force and drag coefficient (C_d), lift force and lift coefficient (C_L) Drag Force & Coefficient of Drag (CD).

The dimensionless coefficient of drag is known as CD. This force coefficient calculates the drag forces acting on the body's flow. This is a crucial element in figuring out how smoothly the body will move as it moves in the opposite direction of the fluid flow. Equation (1) gives a description of the drag force coefficient.

$$C_D = \frac{F_D}{\frac{1}{2}\rho v^2 A} \quad (1)$$

Whereas,

C_D = Drag force coefficient

F_D = Drag Force

ρ = Density of liquid

v = Velocity of fluid

A = Reference area of the body

The lift forces impacting on the body are measured using a force coefficient called coefficient of lift C_L , which has no dimensions and is oriented in the direction of the Y axis. This force assists the body in moving upward, acting in the opposite direction to the body's weight. Equation (2) displays the formula of lift

force coefficient.

$$C_L = \frac{F_L}{\frac{1}{2}\rho v^2 A} \quad (2)$$

Whereas C_L is Lift force coefficient and F_L is Lift Force, ρ Density of liquid, v Velocity of fluid, A Reference area of the body.

3.3 Post Processing

Post processing of any CFD solver is crucial stage. To understand the physics and all the variables' values post processing produces eye catching results. Post-processing in STAR-CCM+ simulation software encompasses a suite of powerful tools designed to analyse, visualize, and interpret simulation results. With a user-friendly interface and extensive capabilities, post-processing enables users to extract valuable insights from their simulations quickly and efficiently. Users can generate a wide range of visualizations, including contour plots, vector plots, streamlines, and particle traces, to visualize key flow variables such as velocity, pressure, temperature, and turbulence. Additionally, post-processing tools allow for advanced data analysis, including statistical analysis, surface integrals, and volume integrals, enabling users to quantify important engineering metrics and performance indicators. With the ability to customize plots, generate animations, and create comprehensive reports, post-processing in STAR-CCM+ facilitates in-depth analysis and effective communication of simulation results, empowering users to make informed decisions and drive innovation in engineering design and analysis processes. In STARCCM+ solver following post processing modules could be used.

3.3.1 Reports

Reports are used to measure a variable value at any specified location or any specified time. Two axis represent the variable either in spatial coordinate or time coordinates. Reports are usually being defined as separate node in star solver which could activated by choosing the appropriate field function and on horizontal axis selection could be made based on time or spatial direction. Reports in STAR-CCM+ simulation software offer a comprehensive means of documenting and presenting simulation results and analyses. These reports serve as a crucial tool for communicating findings, insights, and recommendations to stakeholders and collaborators. With STAR-CCM+'s versatile reporting capabilities, users can create customized reports that include detailed descriptions of simulation setup, boundary conditions, and solver settings, as well as visual

representations of results such as contour plots, streamlines, and particle tracks. Additionally, reports can incorporate tabulated data, charts, and graphs to provide a clear and concise summary of simulation outcomes. Furthermore, STAR-CCM+'s interactive report viewer allows recipients to explore simulation results interactively, facilitating deeper understanding and engagement with the data. Overall, reports in STAR-CCM+ play a vital role in streamlining communication, facilitating decision-making, and driving innovation in engineering design and analysis processes.

3.3.2 Monitors

Monitors are used to store the history of available calculated data from the report. Monitors could adjoin as well to give better understanding of data representation. Monitors are based on two variables. Time which is actually known as time monitor while other is space monitor. Monitors in STAR-CCM+ simulation software serve as powerful tools for tracking and analysing key parameters during the simulation process. These monitors enable users to define specific quantities of interest, such as flow velocity, pressure, temperature, or turbulence intensity, and monitor their evolution over time or across different regions of the computational domain. With real-time feedback, users can assess the convergence of the simulation, diagnose potential issues, and make informed decisions to optimize solver settings or adjust boundary conditions. Monitors also facilitate the identification of critical events or phenomena during the simulation, allowing users to set triggers for alerts or automatically pause the simulation when certain criteria are met. Overall, monitors in STAR-CCM+ provide users with invaluable insights into the behaviour of their simulations, enhancing efficiency, accuracy, and productivity in engineering analysis and design processes.

3.3.3 Scenes

Scenes are graphical visualization of the variables and colour schemes which are used to provide graphical aid to the user. There are different types of scenes which could be used for this representation such as scalar scene in which any scalar variable is used to show its variability while vector scenes are used to create representation of vectors quantities such as velocity field, forces field, EM field lines etc. Scenes in STAR-CCM+ simulation software offer a dynamic and visually immersive means of analysing and presenting simulation results. These scenes allow users to create customized visualizations by combining various elements such as geometry, mesh, results data, and annotations. With intuitive drag-and-drop functionality, users can manipulate objects,

adjust viewpoints, and add visual enhancements to effectively convey complex engineering phenomena. Scenes enable users to explore simulation results in depth, facilitating the identification of trends, patterns, and insights that may not be apparent from raw data alone. Furthermore, scenes can be saved and shared with collaborators, providing a cohesive and interactive platform for communication and collaboration. Overall, scenes in STAR-CCM+ empower users to communicate their findings effectively, enhance understanding, and drive informed decision-making in engineering analysis and design processes.

3.4 Fast Fourier Transform (FFT) Plots

In STAR-CCM+, the extraction of sound pressure level (SPL) values from pressure sensor data involves a multifaceted process that incorporates both fluid flow simulation results and acoustics post-processing tools, including Fast Fourier Transform (FFT) analysis. Initially, pressure sensors are strategically positioned within the computational domain to capture pressure fluctuations resulting from fluid flow. These sensors continuously record pressure data throughout the simulation. Once the simulation concludes, the pressure data collected by the sensors is exported to the post-processing environment. In the post-processing phase, the pressure data undergoes FFT analysis to convert it from the time domain to the frequency domain. FFT analysis decomposes the pressure signal into its constituent frequency components, revealing the spectral content of the acoustic field. By computing the FFT of the pressure data, users can identify dominant frequency components associated with noise sources and assess their contributions to the overall acoustic environment. Subsequently, specialized acoustics analysis tools in STAR-CCM+ are employed to compute SPL values based on the frequency-domain pressure data obtained from FFT analysis. The weighted frequency-domain pressure data is then integrated over frequency bands to obtain SPL values at each sensor location.

STAR-CCM+ provides capabilities for spatial interpolation and visualization, enabling users to interpolate SPL values between sensor locations and generate contour plots or heat maps of acoustic levels throughout the computational domain. This facilitates the identification of areas with high noise intensity and enables engineers and researchers to assess the impact of design changes or operating conditions on acoustic performance. Overall, the extraction of SPL values from pressure sensor data in STAR-CCM+ involves a comprehensive approach that integrates fluid flow simulation results, FFT analysis, and advanced acoustics post-processing tools. This

process enables users to accurately quantify and visualize acoustic levels, facilitating the optimization of designs and the mitigation of noise emissions in various engineering applications.

Chapter 4: Validation

Validation is a pivotal aspect of research, serving as a critical step to confirm the accuracy, reliability, and relevance of research findings. Through validation, researchers verify the integrity of their methods, measurements, data, and results, ensuring that they are free from errors, biases, or inconsistencies. By subjecting research outcomes to rigorous validation procedures, the credibility and trustworthiness of research work gets enhanced, promoting its acceptance and respect within the scientific community. Validation also facilitates reproducibility and replicability, enabling others to verify and build upon existing findings, thus advancing the collective body of knowledge in the field. Furthermore, validation ensures the generalizability and applicability of research findings across diverse contexts or populations, contributing to evidence-based decision-making and the development of effective solutions to real-world problems. Overall, validation is essential for upholding the integrity and quality of scientific inquiry, driving progress and innovation in research endeavors. The validation case is comparison of underwater cylindrical body total resistance to model results, as well as comparing acoustic results to other numerical acoustic result from the literature. In this research work validation is considered one of most important aspects as authentic data pertaining to cylindrical body's hydroacoustic analysis were rarely available in past research works. Considering the novelty of subject, closely resembled bodies were thoroughly searched in past research work having both hydrodynamic and hydroacoustic data available. Research work on DARPA Suboff was taken into consideration as a lot of research work was readily available which could help in developing a valid CFD setup.

4.1 Drag Validation of DARPA Suboff:

Validation is started with the resistance data of the model with the experimental study of Liu & Huang [123]. Comparisons between the well-known form and case of DARPA Suboff experiments and the CFD setup and findings obtained with the STAR-CCM+ are made as part of the validation process. The DARPA Suboff hull is 4.356 meters long and 0.508 meters wide. The DARPA Suboff Configuration 8 (Hull with sail and four stern appendages) and Stern Configuration 3 are used for results comparison. 3.05 m/s or 5.93 knots is used as the reference speed. Fig 4.1 depicts top view of DARPA Suboff .

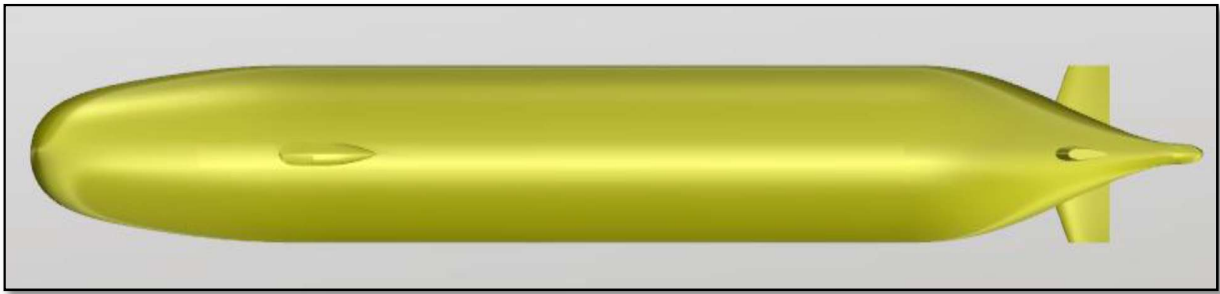


Figure 4.1: Top View of DARPA Suboff.

4.1.1 Mesh Independence Study

The convergence study was conducted by computing the drag for various cell counts to ascertain the impact of cells on the simulation results. For the mesh independence study, the drag was calculated for different base sizes. With the decrease in base size, mesh density increases, and vice versa. The number of cells for different base sizes is given in Table 4-1.

Table 0.1: Mesh density w.r.t base size

Base Size(m)	No of Cells	Grid Density
0.08	1498967	Very Fine
0.1	1211879	Fine
0.12	1051779	Slightly Medium
0.14	980621	Medium
0.1	796789	Slightly Coarse
0.16	574790	Coarse

High-quality mesh generation is one of the most important aspects that should be taken into account to ensure simulation accuracy. It directly affects the accuracy of results, convergence, and time. STAR-CCM+ provides us to create unstructured and structured grid generation. The convergence study in table 4.1 and figure 4.4 shows the simulated results for the drag converging after 1.2 million cells with fine meshing. So, a base size of 0.1m was used for further simulations. Figure 4.2 & 4.3 depicts mesh view and scaler aspect w.r.t velocity of DARPA Suboff.

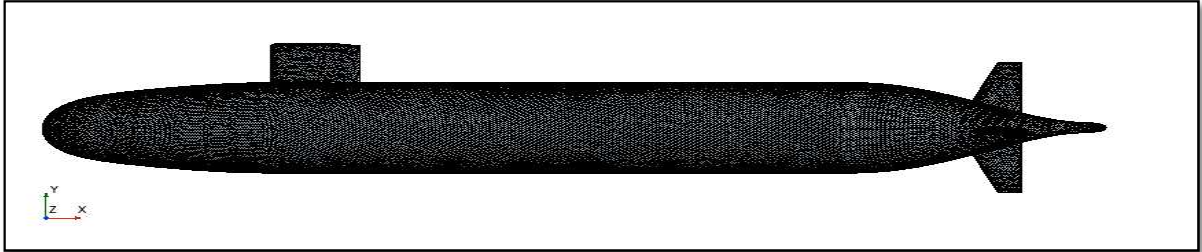


Figure 4.2: Mesh View of DARPA Suboff.

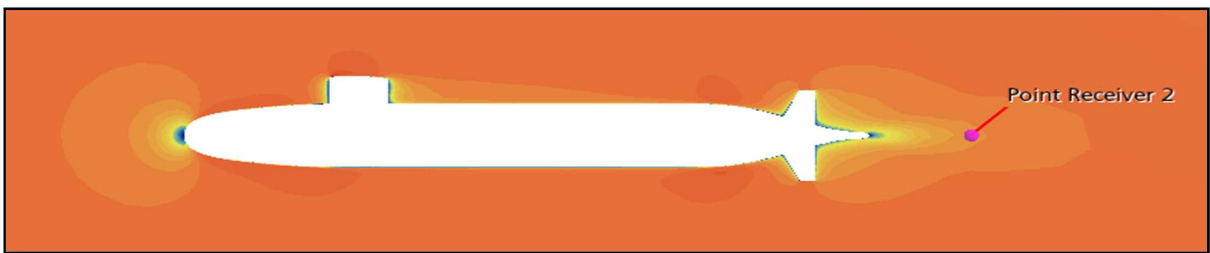


Figure 4.3: Scaler scene (Velocity magnitude) of DARPA Suboff.

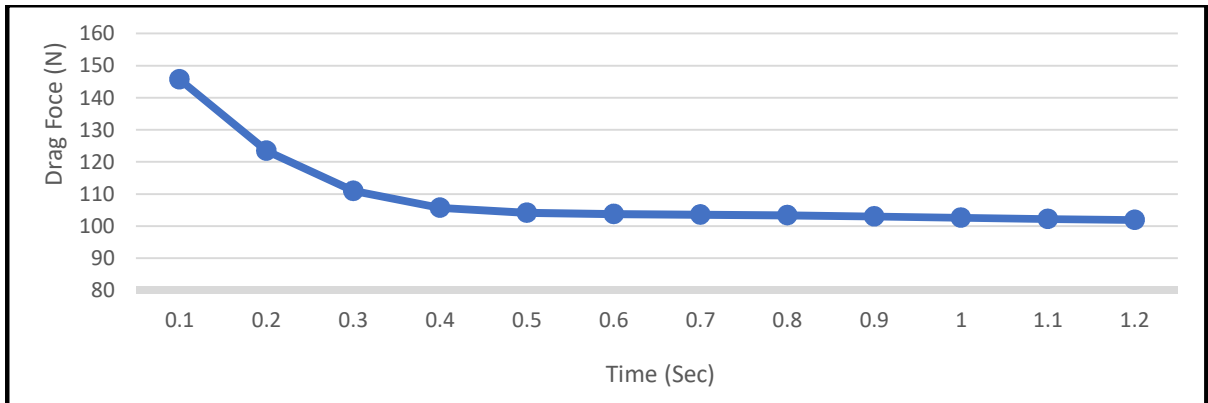


Figure 4.4: Calculated DARPA Suboff Drag.

Table 4.2: Comparison of the CFD results with the experiment

Model Speed [m/s]	Total Resistance (CFD Calculated) [N]	Total Resistance (Experiment) [N]	Relative Error [%]
3.05	101.86	102.30	0.42%

4.1.2 Acoustics Validation with results of H. Yao et al., 2017

By solving the FW-H equations, the flow noise of the DARPA Suboff with a velocity of 3.05 m/s is compared to the results of H. Yao et al., 2017 [124]. The acoustic values are predicted using STAR-CCM+. Noise is initially predicted in the time domain. Pressure time series are used to record the results. The Fast Fourier Transform (FFT) is used to calculate the undersea radiated noise. The frequency domain acoustic data that was gathered throughout the simulation is created via FFT from the time domain data. The FFT's time period is selected based on convergence and flow characteristics. To the FFT data, a discrete probability function is used. The spectral data can reach up to 10,000 Hertz when time step 5E-5 is used. Below are the calculated spectra of the DARPA Suboff's flow noise using FW-H using STAR-CCM+:

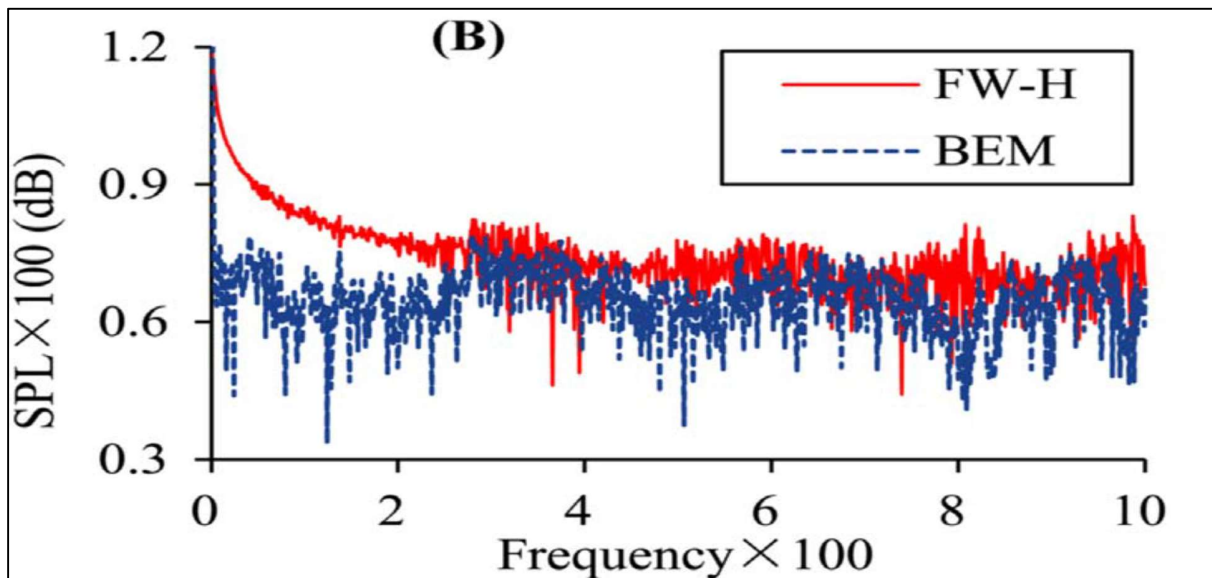


Figure 4.5: Flow noise of the DARPA Suboff by (H. Yao et al., 2017) using FW-H and BEM.

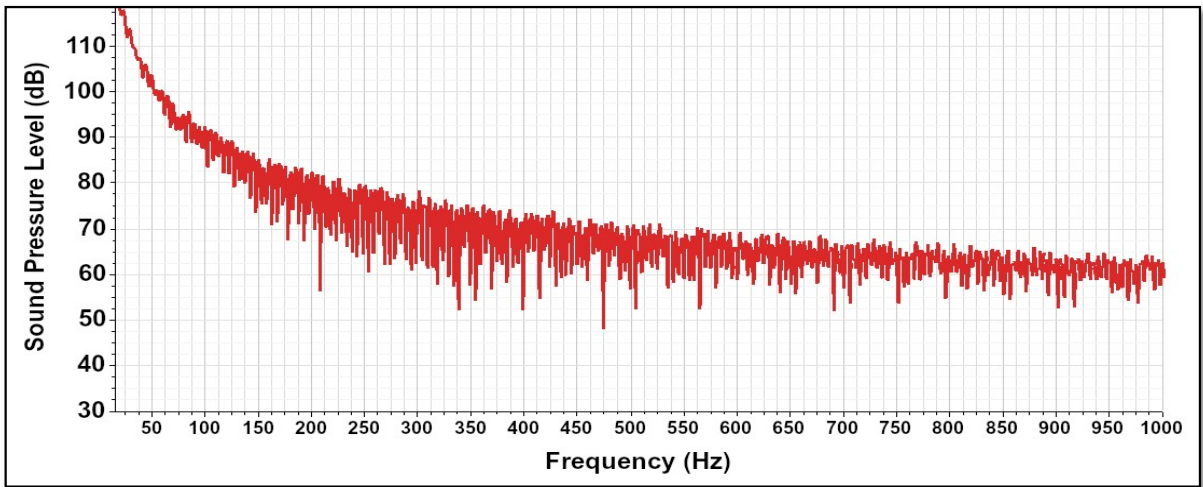


Figure 4.6: Calculated Flow noise of the DARPA Suboff using FW-H (CFD).

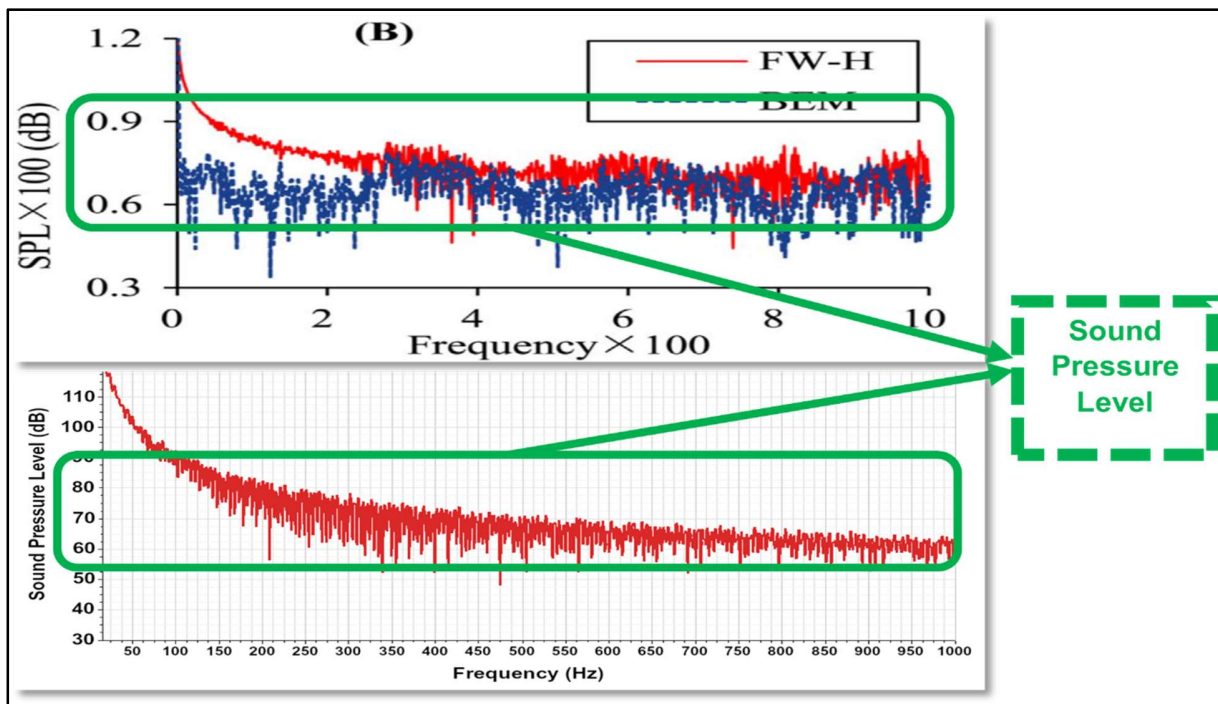


Figure 4.7: Comparison of Flow noise of the DARPA Suboff with results of H. Yao et al., 2017

Figure 4.7 depicts almost similar trends of acoustics against different frequencies when compared with literature data shown in fig 4.5. Observed miniature Variance in data is due computational and time limitation. Actual data obtained at fig 4.6 is attached here in case of acoustics simulation,

however for final report graph plotting using different tools will be considered to depict both experimental and literature results.

4.2 Acoustics Validation with K Karthik et al., 2020 on Cylindrical shaped under water body

Research work by K Karthik et al., 2020 was found relevant to scope of this research work. The long and thin array has a length (L) of 12 m and diameter (D) of 10 mm velocity at inlet is 5 Kn. After basic understanding of steps leading to acoustic simulation, relevant literature was thoroughly studied and research work by K Karthik et al., 2020 [125] was found relevant to scope of this research work. Drag and flow noise of the body with 10 mm diameter and 12 m length as shown in fig 4.8 was calculated and results were compared.

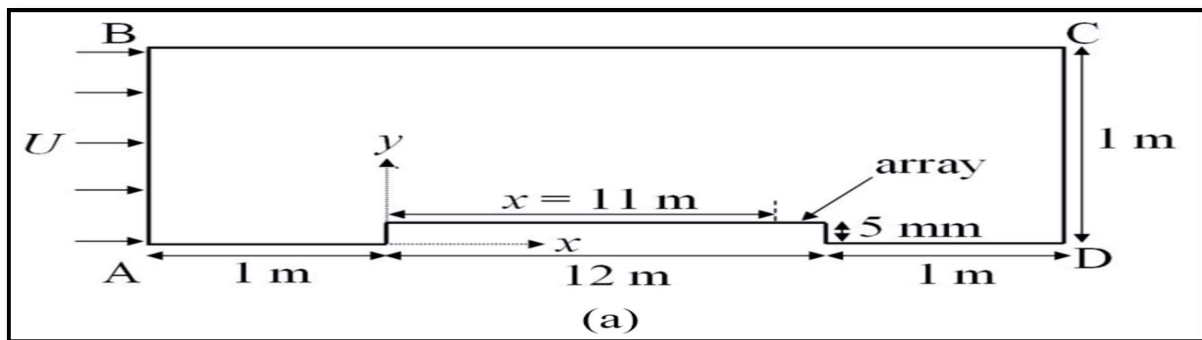


Figure 4.8: Depiction of underwater body in domain

In the context of my research paper, the comparison graph at fig depicting sound pressure level versus frequency assumes a critical role in validating the integrity of my findings. Its incorporation validates the robustness of my methodology and the precision of my measurements, reinforcing the credibility of my research outcomes. The coherent relationship observed between sound pressure level and frequency not only confirms the hypotheses I've formulated but also provides empirical substantiation for the theoretical framework driving my study. Moreover, this graph serves as a visual representation of the trends and patterns I've discerned through my simulation work and analysis. By clearly illustrating the nearly similar trend between sound pressure level and frequency, it offers compelling evidence of a consistent relationship between these variables. This not only bolsters the validity of my conclusions but also strengthens the persuasiveness of my arguments within the scientific community.

Furthermore, the inclusion of this comparison graph at fig 4.9 underscores the significance of robust validation in scientific inquiry. By rigorously scrutinizing and validating my results through empirical evidence, ensure the reliability and trustworthiness of my findings. This not only enhances the credibility of my research paper but also contributes to the broader scientific discourse by advancing our understanding of acoustics and sound propagation phenomena.

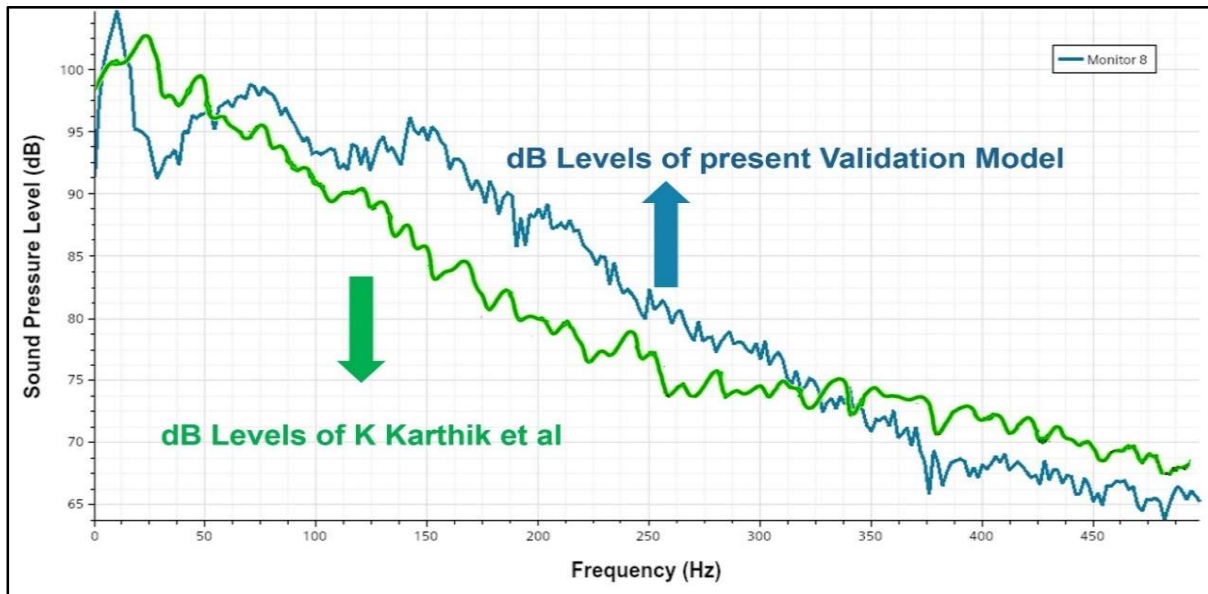


Figure 4.9: Comparison with obtained Results of K Karthik et al., 2020

In essence, the comparison graph of sound pressure level versus frequency plays an instrumental role in validating my setup, providing empirical support for my hypotheses and enhancing the overall credibility and significance of my study.

4.3 Outcomes of validation work:

Considering DARPA Suboff for acoustic simulation also revealed that drag validation of body also validates its acoustics results as well. As after validation of drag of a body not much changes are incorporated in setup i.e applying pressure sensors at certain location and then extracting data from those sensors verses time. The Fast Fourier Transform (FFT) is then used to analyze the hydro acoustics. The frequency domain alone is obtained using FFT from the time domain acoustic data that was gathered during the simulation.

Chapter 5 Simulations

After carrying out validation work Dedicated Simulations were then started considering available computation resources. Considering the computation limitation bodies of smaller length were considered and complete acoustic analyses were carried out. Bodies with dias of 10, 25 and 50 mm and length of 0.4 m were considered. Simulations were carried out on 2 different velocities (3m/sec and 5 m/sec). Initially RANS were utilized but later on simulation were also carried out using LES (Large Eddy Simulation). Results obtained from LES were considerably better than RANS w.r.t acoustic depiction. The methodology for carrying out simulation work and for achievement of desired result following research methodology shown in fig 5.1 is being followed.

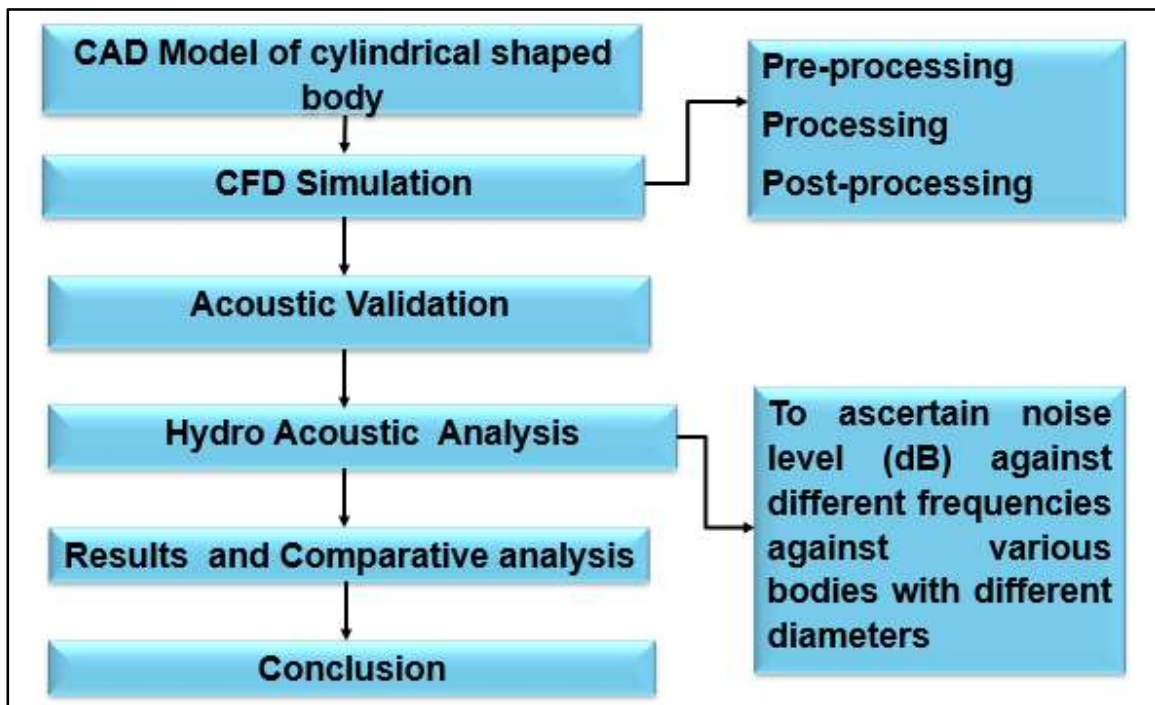


Figure 5.1: Research Methodology

5.1 Modeling

After the completion of the validation models with the DARPA Suboff and Kartik, modelling of underwater cylindrical shaped bodies is started. Solid Works software is used for model preparation. Model of the Cylindrical shaped bodies having diameter of 10 , 25, 50 mm can be seen in Figure 5.1

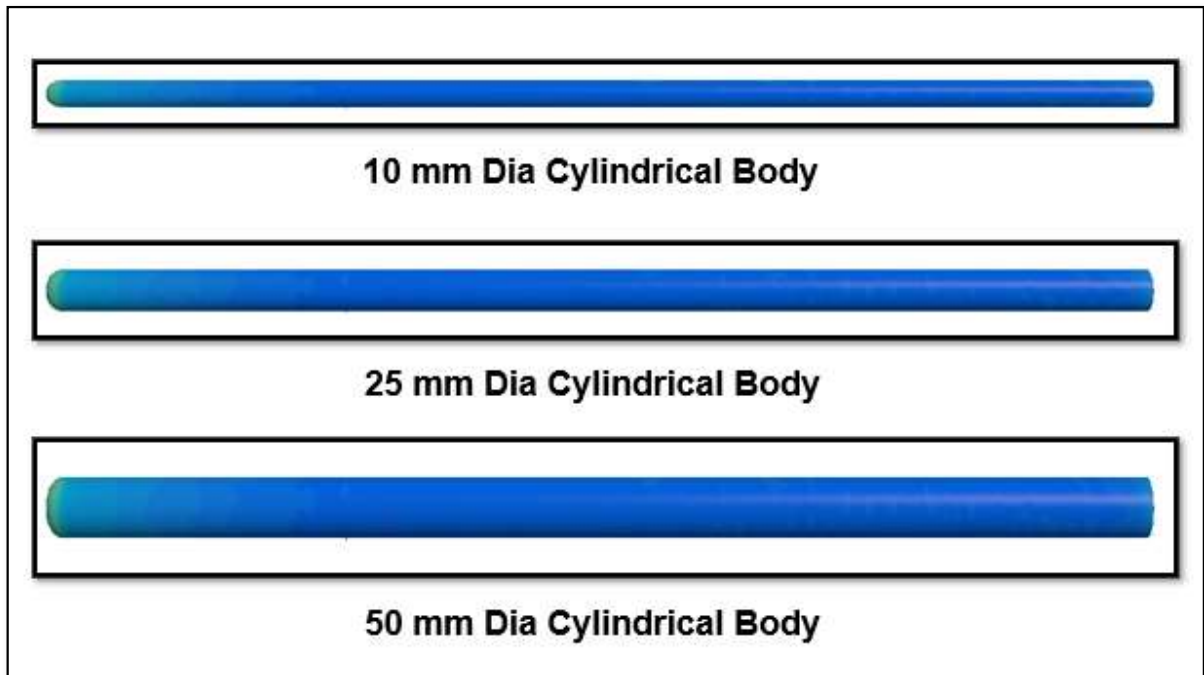


Figure 5.2: Under water cylindrical shaped bodies with diameter of 50, 25, 10 mm.

5.2 Computational Domain

Initially the three-dimensional body displayed in figure 02 (a) above was designed in Solid Works. To perform a CFD simulation, the body must be imported as an IGES file into Star CCM+. After the model was imported, the computational domain was set up. Block and Cylinder make up the computational domain. The cylinder was placed for refinement purpose around the body only whereas the block was considered motionless part. Boundary conditions have been defined through developing a computational domain and using a function split by patch to denote the block's inlet, outlet, and symmetry conditions. The inlet was regarded as the velocity inlet. Because of the static pressure conditions at the outflow boundary, the exit was assumed as a pressure outlet. At the sides, top, and bottom of whole domain, symmetry conditions have been considered. Subject body was regarded as a no-slip case. Figure 5.3 & 5.4 displays a magnified image of complete computational domain and the boundary conditions that were considered.

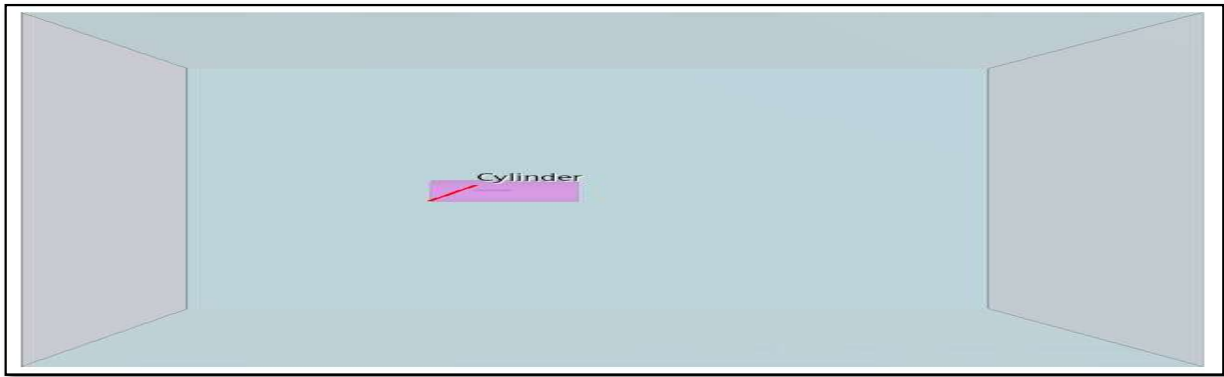


Figure 5.3: Domain of the underwater cylindrical shaped body.

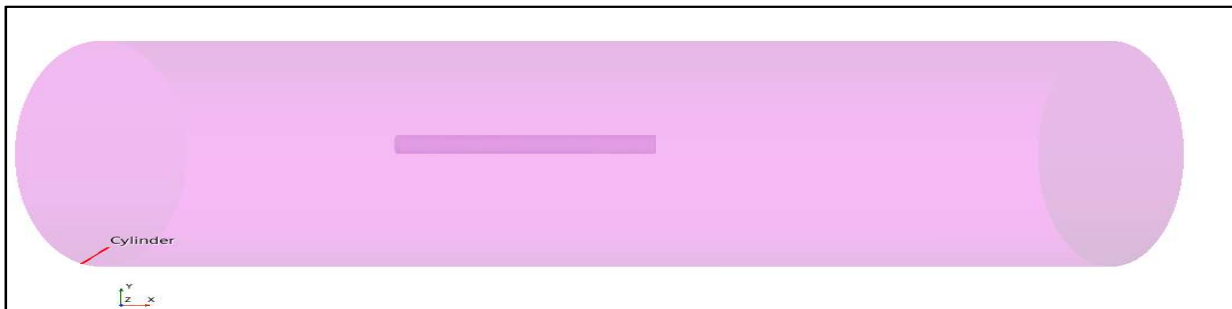


Figure 5.4: Refined Cylindrical Domain of underwater cylindrical shaped body.

5.3 Boundary Conditions

Boundary conditions are essential to CFD as they define the flow direction of stream parameters like energy, mass, and momentum between other variables. Before starting the simulation, the following boundary conditions have been identified. Table 04 shows the parameters set up before the simulation.

Table 5.1: Boundary Conditions

Reference Parameters	Reference Values
Inlet Velocities	3.05 & 5.05 m/sec
Pressure	101325 Pa
Density	997.561 kg/m ³
Dynamic Viscosity	0.00088871 Pa sec

5.4 Physics Conditions

The basic parameters of the simulation (such as pressure and velocity) are specified by physics models, together with the mathematical procedure that is used to generate the solution. A suitable set of models must be combined to fully define a physics continuum. A physics continuum (such air, water, etc.) contains the models used to depict the flow of the selected fluid. In the present study, water (a liquid) is the chosen fluid flow because of its turbulent nature.

The parameters that were required after the meshing setting was finished are listed below.

- All y^+ wall treatment
- Constant density liquid (Water)
- Unsteady
- Three dimensional
- Segregated flow
- Reynolds-Averaged Navier-Stokes & Large Eddy Simulations
- Turbulent
- Aeroacoustics
- Ffowes Williams-Hawkings Unsteady

Because it is a single-phase fluid, water was chosen. The SST $k-\omega$ model was enabled and the turbulent condition was chosen based on the segregated flow's fluid flow features. SST $k-\omega$ was selected since it is a hybrid model that includes both $k-\omega$ and $k-\epsilon$. The flow closest to the wall is most effectively expressed by $k-\omega$, while the flow farthest from the wall is better represented by $k-\epsilon$.

5.5 Meshing

One of the most crucial factors that must be considered to achieve simulation validity is outstanding mesh creation. It has a direct impact on time, convergence, and output correctness. Part base meshing and region base meshing are the two forms of meshing. Part base meshing is employed in this study by using Automated Mesh tool in Star CCM+. With the help of part base meshing the computational time has been saved. In contrast to region-based meshing, it defines the procedure from the basic geometry to the finished volume mesh using a sequence of mesh operations. You can change the initial shape and rerun the

entire procedure with no new inputs by using a series of operations. Because of this, parametric design studies are especially well suited to parts-based meshing. In the current study both structured and unstructured grids have been utilized using STAR-CCM+. Surface remesher, trimmed cell mesher, polyhedral and prism layer were all used in computational domain to generate high quality mesh in the current investigation. The volume mesh was created using a trimmed cell mesher since it was particularly effective at converging the solution. Consequently, hexahedral grid cells are used to divide up the entire region being meshed. Furthermore, custom controls were applied to the sail and control surfaces of the body to further improve the mesh. With the help of meshing idea, different values for the base size, surface size, thickness of the prism layer, number of prism layers, surface curvature and other variables have been attempted to produce the refined mesh of complete domain. The mesh depiction is displayed in Figure 5.6 – 5.8. The object's wall is added with prism layers by the prism layer mesher. The exact nature of the flow close to the wall is improved by this layer of cells. Figure 5.9 displays a representation of the prism layer close to the surface of the body.

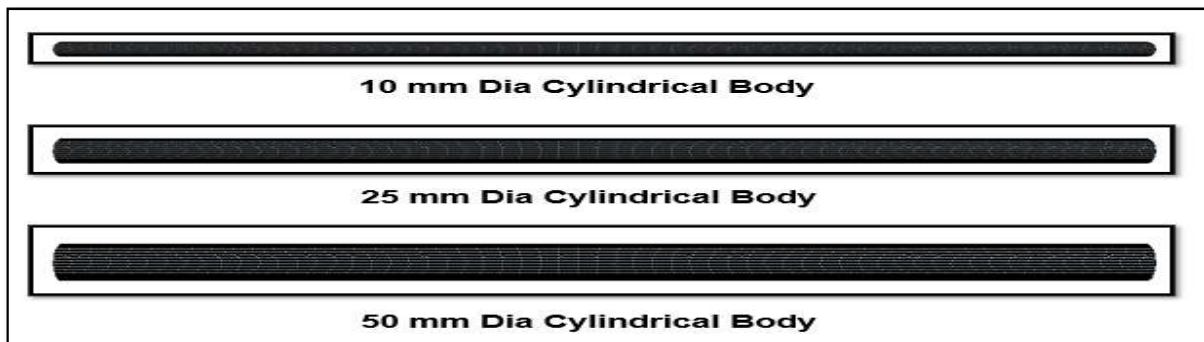


Figure 5.6: Mesh Depiction bodies with 10, 25- & 50 mm diameter

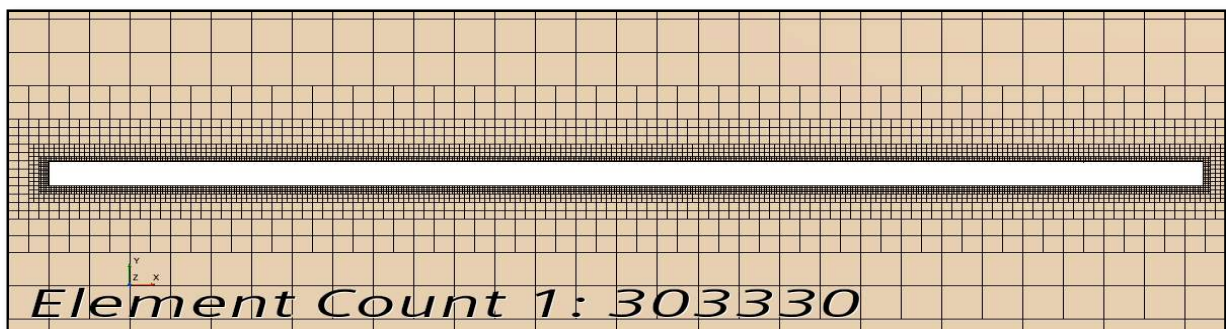


Figure 5.7: Mesh of the refinement zones and surface from top.

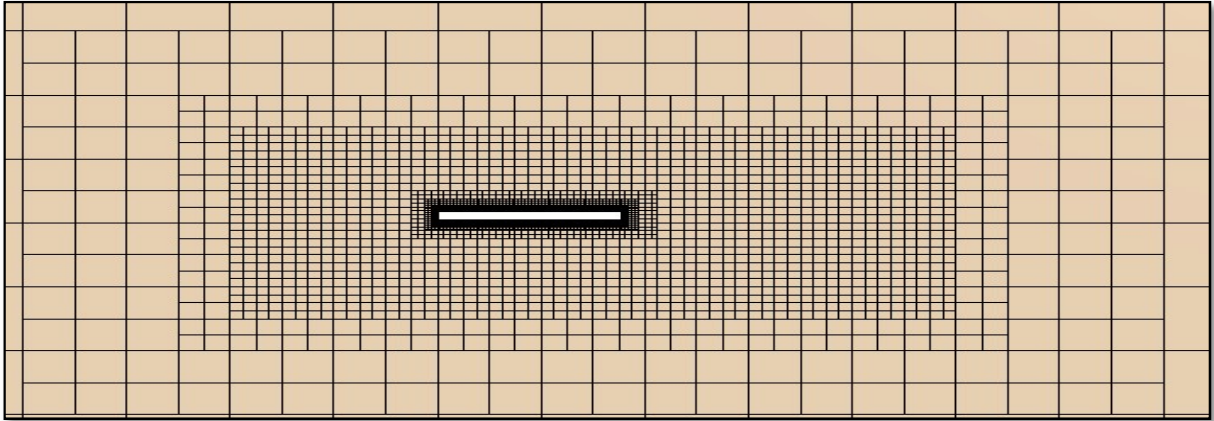


Figure 5.8: Mesh inside of the domain for underwater cylindrical shaped body.

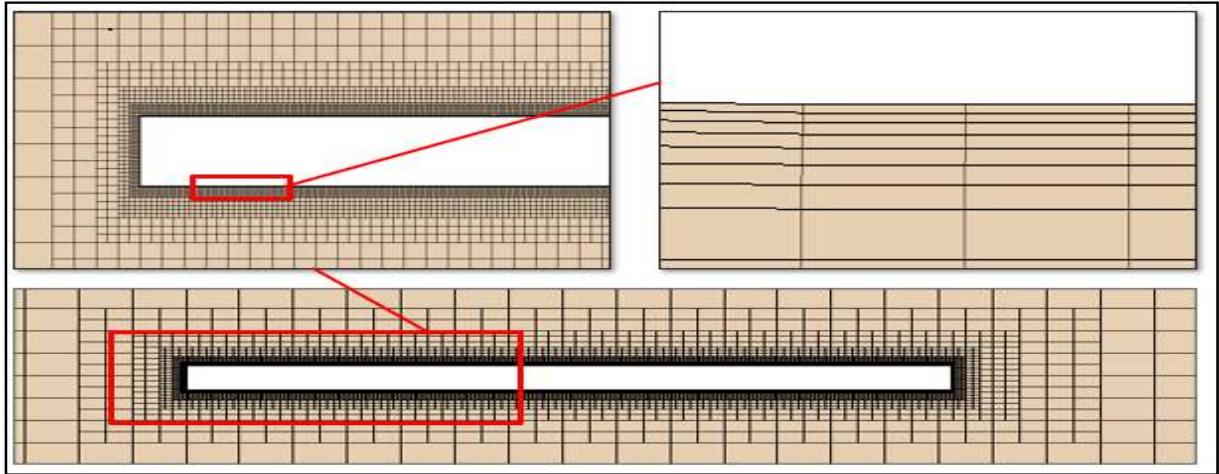


Figure 5.9: Prism layers close to the surface of the body

For all underwater cylindrical-shaped bodies, the same turbulence model, y^+ value, and other CFD parameters are used as the validation case. The URANS family's K-epsilon ($k-\epsilon$) turbulence model is applied. The border layer sets the y^+ value to be around 5. Mesh zones are created using the STAR-CCM+ automatic mesh mesher. Surface Remesher, Trimmed Cell Mesher, and Prism Layer Mesher are the chosen mesh parameters. To expand the computational domain's division, the base size of 0.1 m—a number that differs from the validation case—was used. Refinement zone dimensions, however, are chosen differently to accommodate all components while maintaining these zones parallel to the flow. Without influencing the outcomes of the computation, minimum dimensions are attempted to be chosen. These configurations result in a total cell number for the case of 0.3M at 10 mm diameter, 0.34M at 25 mm diameter, and

0.4M at 50 mm diameter with a fluid density of 998.2 kg/m³ and a dynamic viscosity of 0.001003 Pa-s, a constant density assumption is assumed. chosen fluid to be Newtonian. 3.05 m/s is the chosen flow velocity in the positive x direction. Using these values in the calculation, the Reynolds Number for the examples comes out to be 2.8E6. The simulation's time step is set at 0.001 in order to maintain a frequency range of up to 1000 Hertz, and the inner calculation iteration is set to 3 in all circumstances.

5.6 Virtual Hydrophones

Pressure data is retrieved in pa using virtual hydrophones positioned at different distances from the subject's body. Hydrophones extend in the x, y, and z directions and are situated close to the body. Hydrophones lie in the z direction and only extend to the positive z side due to the symmetry in the XY plane as shown in fig 5.10.

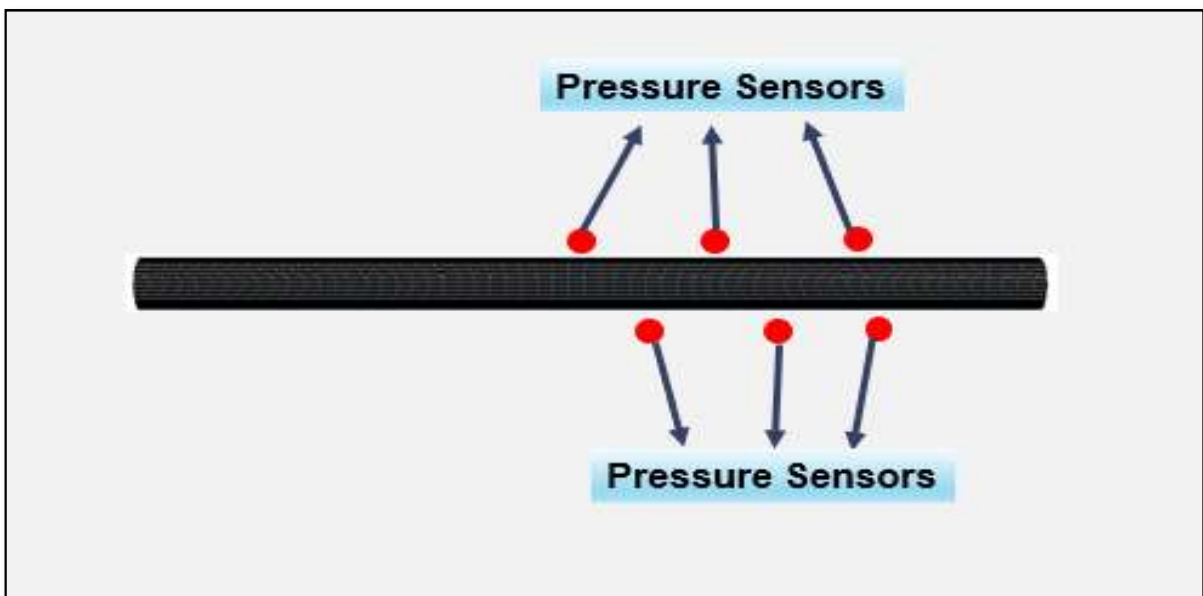


Figure 5.10: Visualization of the virtual hydrophones around the body.

Chapter 6: Results & Discussion

Three distinct diameter possibilities are examined in the analysis of cylindrical body situations. These situations vary when the diameter is changed to 10, 25, or 50 mm. The noise in the placed virtual hydrophones is calculated using the FW-H analogy and the Farassat 1A equation in all circumstances. The RANS and LES turbulence models take k-epsilon into consideration when conjugating with the improved wall treatment model. In order to enable the comparison of various diameters and to compare the noise level including the turbulence parameter/fields, results from virtual hydrophones situated in the turbulence zone are provided. Total Sound Pressure Figure 5.1 shows the level of the points and the hydrophone locations for every angle of attack scenario in the XY plane. These hydrophones are dispersed across the coordinate system in close proximity to the body's surface.

Three noise factors are present in the FW-H analogy: loading, thickness, and quadrupole. In the maritime instances that concentrate on flow noise, the loading (monopole) term is the main source of noise. Over the surface, loading and thickness sound sources develop. Thus, Total Surface is the sum of these two quantities.

After validation of drag and acoustics further analysis work is being conducted. Different pressure sensors were placed near to surface of underwater bodies for all three models. Results were then obtained in form of maximum pressure at those location and subsequently FFT plots were drawn using those maximum pressure values. Figures 6.1 & 6.2 reflect results obtained from pressure sensors. These results determine trend of changing diameter on sound pressure levels. Due to computation and resource constraints, the simulation's time step of 0.001s is chosen to cover the frequency range up to 500 Hertz. However initial results reflected that hydroacoustic trend due diametrical changes is considerably visible at said time step and this time step can be used for further simulation. These results also depict that changing diameter of body reduces sound pressure levels. Further research outcomes can be obtained after detailed analysis.

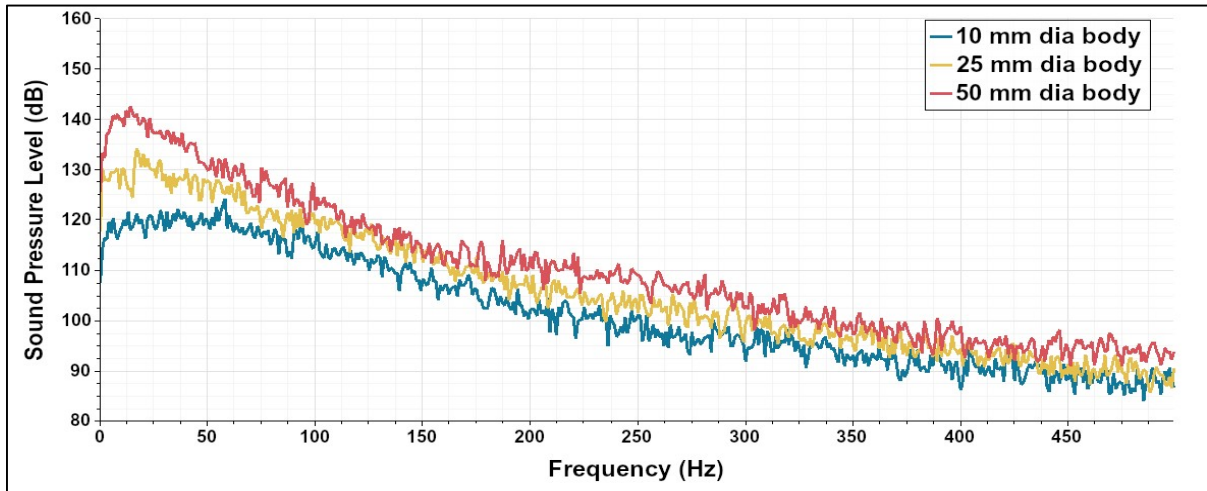


Figure 6.1: Sound Pressure Level Vs Frequency Plot at 3.05 m/sec (Using LES Model)

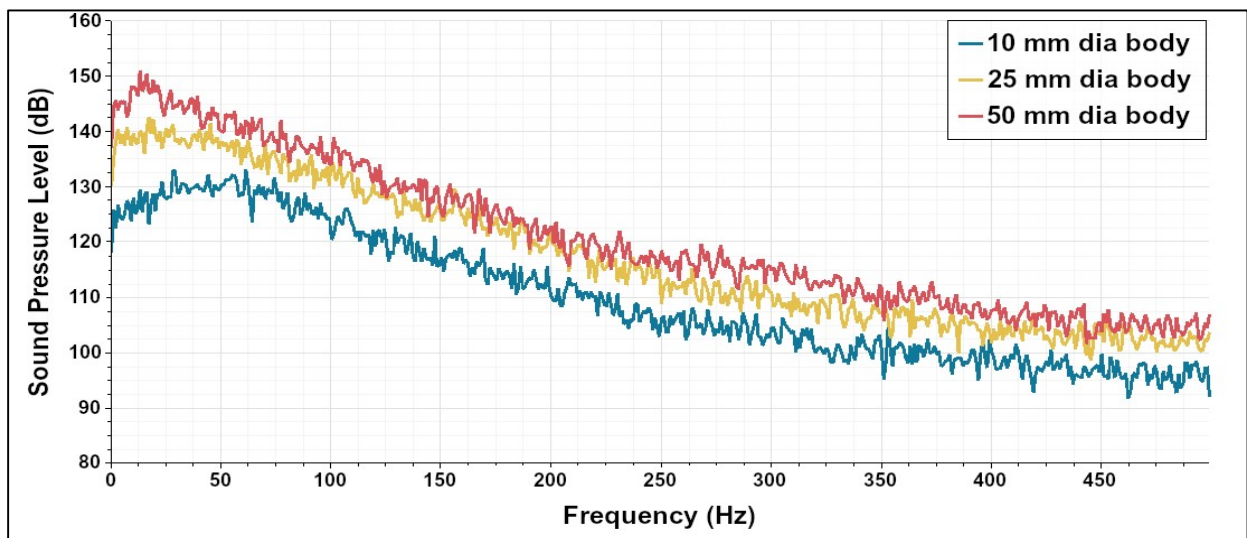


Figure 6.2: Sound Pressure Level Vs Frequency Plot at 5.05 m/sec (Using LES Model)

Both Reynolds-Averaged Navier-Stokes (RANS) and Large Eddy Simulation (LES) are utilized for analyzing underwater hydroacoustic noise, with each approach offering distinct advantages depending on the specific requirements of the analysis.

RANS simulations are commonly employed to predict mean flow properties and averaged noise levels over time. These simulations are computationally less intensive compared to LES and are well-suited for capturing large-scale flow structures in underwater environments. RANS simulations can provide valuable insights into overall flow behavior and help predict noise levels

in scenarios where the flow is predominantly turbulent but not highly unsteady. They are particularly useful for analyzing noise generated by submerged structures or vehicles in relatively steady flow conditions.

Conversely, LES is better suited for capturing unsteady turbulent flow phenomena, which play a significant role in hydroacoustic noise generation in dynamic underwater environments. LES resolves larger turbulent eddies explicitly while modeling smaller ones, allowing for a more accurate representation of the turbulent flow field. This makes LES particularly useful for predicting the turbulent fluctuations that contribute to noise generation in complex flow configurations, such as those encountered in underwater propulsors, turbulent wakes, or flow around underwater structures both fig 6.3 & 6.4 depicts scalar scenes w.r.t. velocity and pressure functions.

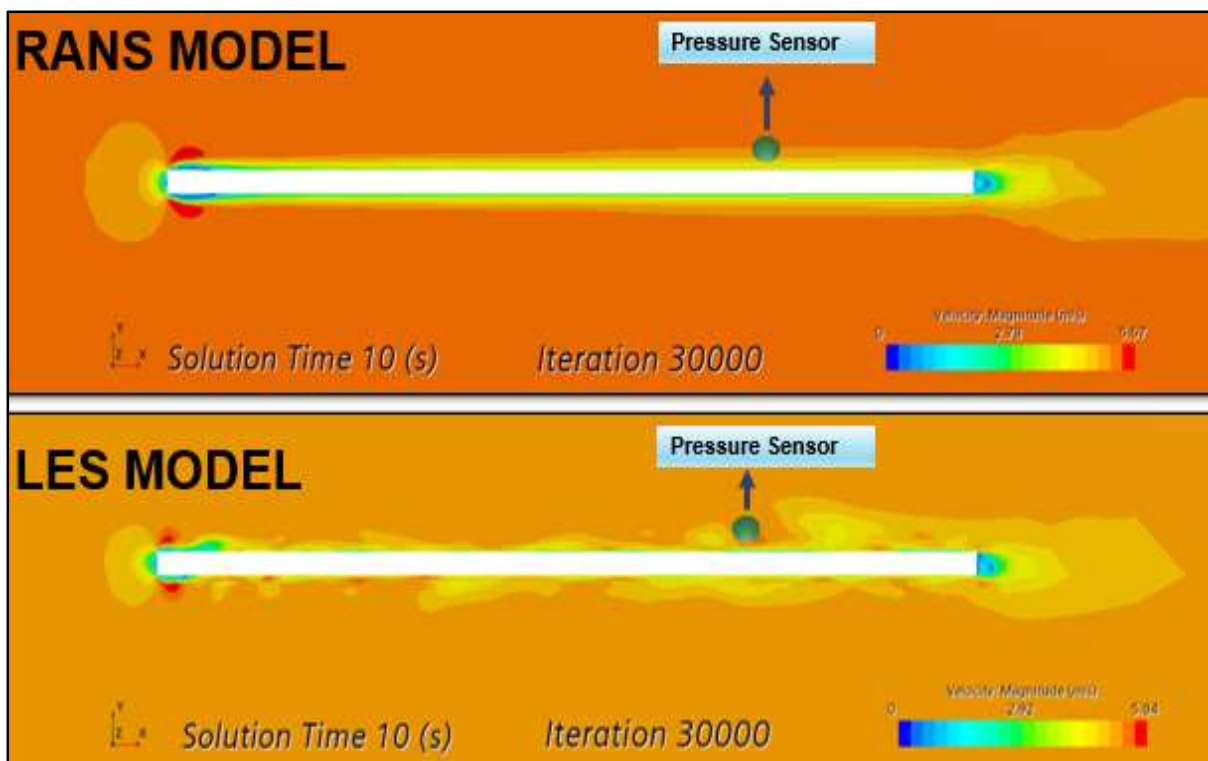


Figure 6.3: Scaler Scenes Comparison (Velocity Function)

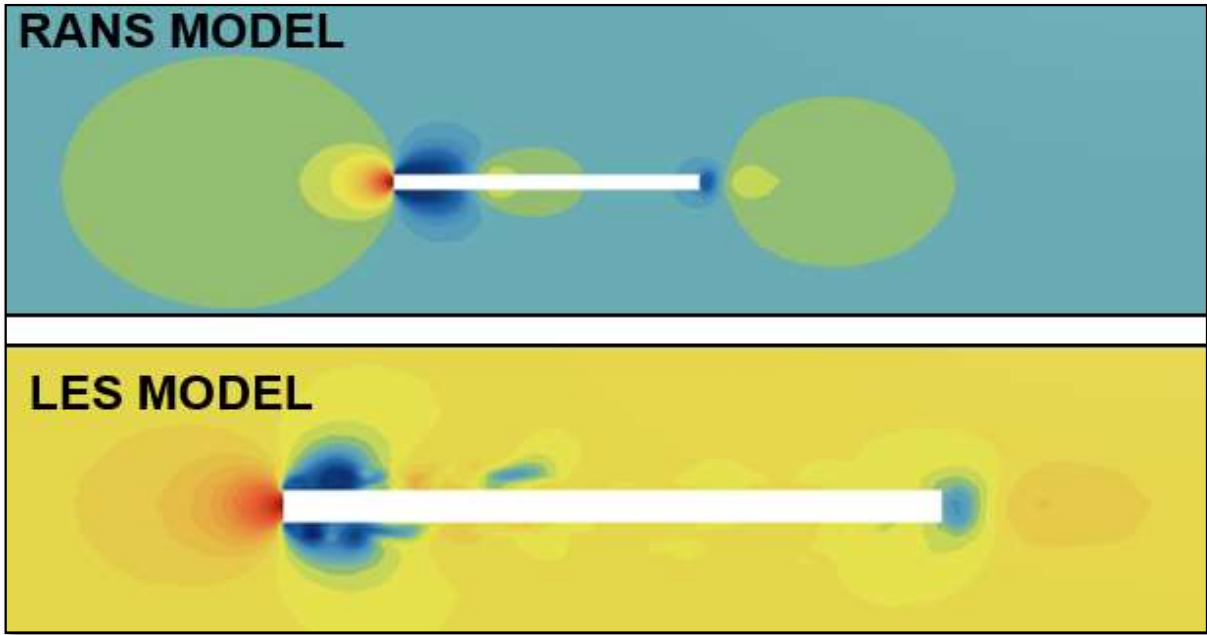


Figure 6.4: Scaler Scenes Comparison (Pressure Function)

The convergence requirements for the CFD analysis depend on the residuals. Four residuals' variables were monitored during the computing process. These factors include continuity, x, y, and z-momentum as shown in figure 6.5.

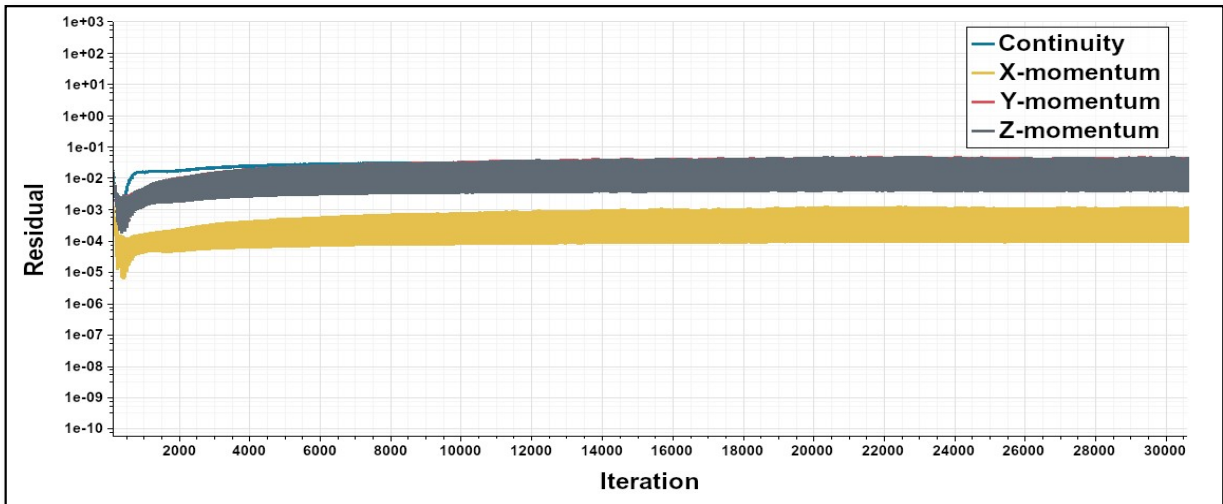


Figure 6.5: Residuals in Continuity, X,Y,Z momentum.

The computational fluid dynamics (CFD) simulations conducted in this study have yielded insightful results concerning the correlation between the diameter of an underwater cylindrical

shaped body and the resultant noise generation. A series of diameters were examined in the simulations, including 50 mm, 25 mm, and 10 mm, representing a spectrum from larger to smaller dimensions. The resultant noise levels were meticulously recorded and analyzed across these configurations. Employing cutting-edge CFD software facilitated precise modeling of fluid flow and acoustic phenomena surrounding the cylindrical body. The outcomes clearly demonstrate a discernible pattern: as the diameter diminishes, so does the generated noise. This trend persisted across all diameters tested, affirming the consistency and reliability of the findings.

The insights gleaned from the CFD simulations offer significant implications for the design optimization of underwater cylindrical shaped bodies to mitigate noise emissions. Across the range of diameters explored (50 mm, 25 mm, and 10 mm), the observed diminution in noise with decreasing diameter aligns with fundamental fluid dynamics principles.

- Primarily, the reduction in diameter curtails the surface area exposed to the surrounding fluid, thereby diminishing turbulence and vorticity, both significant contributors to noise production in fluid flow scenarios. Consequently, noise emissions were markedly attenuated.
- Secondly, the decrease in diameter leads to a concomitant reduction in the cross-sectional area through which fluid traverses, thereby mitigating flow resistance and pressure fluctuations, further mitigating noise levels.

Furthermore, the variation in diameter may instigate alterations in fluid-structure interaction dynamics, influencing the propagation and attenuation of acoustic waves, thereby modulating the overall noise signature of the cylindrical body. The observed noise reduction with diminishing diameter bears profound implications for various applications, including underwater vehicles, marine structures, and offshore installations. By optimizing design parameters, particularly diameter, noise emissions can be minimized, enhancing environmental sustainability and mitigating the deleterious impact on marine ecosystems.

However, it is imperative to acknowledge certain limitations and considerations associated with the findings. The simulations were conducted under specific assumptions and simplifications, warranting further experimental validation to corroborate the results. Additionally, the effects of other design parameters, such as length, shape, and surface properties, necessitate further investigation to comprehensively assess their influence on noise generation. Results derived from the CFD simulations, incorporating diameters of 50 mm, 25 mm, and 10 mm, offer significant

insights into the interplay between diameter and noise emissions for underwater cylindrical shaped bodies. The observed noise reduction with decreasing diameter underscores the potential for design optimization to abate noise pollution in underwater environments. Future research endeavors should prioritize refining the understanding of these intricate fluid dynamics phenomena and exploring additional design parameters to further augment noise reduction strategies. Findings from this research hold significant implications for the future fabrication and optimization of towed array SONAR systems, particularly in terms of noise reduction strategies. Towed array SONAR systems are critical components of underwater surveillance and detection systems, used extensively in naval operations, oceanographic research, and marine resource exploration. These systems comprise an array of hydrophones towed behind a vessel, tasked with detecting and localizing underwater targets by analyzing acoustic signals. One of the primary challenges faced in towed array SONAR systems is the mitigation of self-noise, generated by the hydrophones and associated mechanical structures as they move through the water. The noise generated by the towed array can significantly interfere with the detection of faint acoustic signals from distant targets, thereby compromising the system's effectiveness.

The research findings demonstrating a reduction in noise with decreasing diameter of cylindrical shaped bodies have direct relevance to the design and fabrication of hydrophones and other components within towed array SONAR systems. By incorporating smaller diameter components, engineers can potentially minimize self-noise levels, enhancing the system's sensitivity and detection capabilities.

Advanced materials with tailored acoustic properties could be utilized to fabricate hydrophones and structural components, minimizing vibration and turbulence-induced noise. Moreover, the optimization of towed array configurations based on the principles elucidated in this research could lead to more efficient and compact systems. By strategically arranging smaller diameter hydrophones within the array, we can potentially enhance acoustic performance while reducing overall system size and weight, offering logistical and operational benefits. Additionally, the findings may stimulate further research into the integration of active noise control techniques within towed array SONAR systems. By leveraging real-time feedback and adaptive algorithms, active noise cancellation systems could actively suppress self-noise generated by the array, further enhancing detection capabilities in challenging acoustic environments.

Chapter 7: Conclusion and Future Prospect

7.1 Conclusion

Through meticulous CFD modeling and analysis, this research work has uncovered a significant correlation: decreasing the diameter of cylindrical bodies results in a marked reduction in flow noise, offering pertinent implications for various applications in underwater acoustics. Numerous turbulence flow models have been discussed. The advantages, implementations, and discrepancies of different models have been given. Also, the usage of hybrid models for hydroacoustic noise prediction has been reviewed. Furthermore, the use of software tools for acoustic analysis such as STAR-CCM+ has been investigated. The acoustic properties of an underwater body with a cylindrical form are examined in this thesis. Computational fluid dynamics methods are used to execute simulations. Additionally, hydrodynamic characteristics such as pressure, turbulent kinetic energy, vorticity, and velocity affect the acoustic outcomes as well as the size of the sound source type under study. Total surface noise is computed using the Farassat 1A formulation and the FW-H acoustic analogy. One of the key factors in the acoustic measurement of flow noise is turbulence, which is modeled using the improved wall treatment model and the k-epsilon turbulence model from the RANS and LES turbulence model families. Underwater cylindrical bodies travel between 3.05 and 5.05 meters per second. The impact of different cylindrical bodies with different diameter on hydroacoustic noise prediction has been examined. This research provides essential data for comprehending how geometric factors affect the hydroacoustic properties of underwater cylindrical shaped structures. Moreover, this research offers valuable insights and avenues for innovation in the fabrication and optimization of towed array SONAR systems. By leveraging the demonstrated benefits of reducing diameter to mitigate noise emissions, future advancements in towed array technology can enhance underwater surveillance, navigation, and scientific exploration capabilities, contributing to the broader goals of marine security and environmental monitoring. CFD-based approach employed in this study serves as a foundation for future research endeavors aimed at refining noise reduction strategies and optimizing design parameters. By advancing CFD techniques and modeling approaches, researchers can continue to explore the complex dynamics of underwater acoustics and develop innovative solutions to address real-world challenges effectively. CFD simulations conducted in this study represent a significant contribution to the field of underwater acoustics, providing

actionable insights that have the potential to drive advancements in engineering practices and environmental conservation efforts.

7.2 Future Prospect

The research conducted on the correlation between diameter reduction and noise attenuation in underwater cylindrical shaped bodies holds promising future prospects in various fields of underwater acoustic technologies. As the understanding of fluid dynamics and noise propagation continues to evolve, several potential avenues for future research and application emerge. Machine learning applications can be incorporated into hydroacoustic noise prediction. The research findings on the correlation between diameter reduction and noise attenuation in underwater cylindrical shaped bodies hold promising future prospects, especially with the integration of machine learning and artificial intelligence (AI). As advancements in underwater acoustic technologies continue to evolve, machine learning algorithms could play a pivotal role in optimizing design parameters and predicting noise reduction outcomes with greater accuracy. By leveraging AI-driven simulations and data analytics, engineers and researchers can explore complex fluid dynamics phenomena and identify optimal configurations for noise mitigation. Additionally, machine learning techniques could be applied to develop intelligent noise cancellation systems that adapt in real-time to changing environmental conditions, further enhancing noise reduction capabilities. Interdisciplinary collaborations between acoustics experts, data scientists, and AI experts could lead to innovative solutions that revolutionize underwater engineering practices, environmental conservation efforts, and education outreach initiatives. By harnessing the power of machine learning and AI, the research opens up new frontiers for advancing underwater acoustic technologies and addressing pressing environmental challenges in marine ecosystem. The impact of different cylindrical bodies especially while considering application of towed array SONAR and the impact of dimensions such as diameter, aspect ratio, and side ratio on hydroacoustic noise prediction can be investigated in the future with more detail. The interdisciplinary nature of the research opens up possibilities for collaboration with other fields, such as material science, fluid dynamics, and signal processing. Future research could explore synergies between noise reduction techniques and advancements in materials science to develop novel acoustic materials with tailored properties for underwater applications.

References

- [1] M. E. Yildizdag, I. T. Ardic, M. Demirtas, and A. Ergin, "Hydroelastic vibration analysis of plates partially submerged in a fluid with an isogeometric FE-BE approach," *Ocean Engineering*, vol. 172, pp. 316-329, 2019.
- [2] A. del Toro Llorens and J. Kiendl, "An isogeometric finite element-boundary element approach for the vibration analysis of submerged thin-walled structures," *Computers & Structures*, vol. 256, p. 106636, 2021.
- [3] Y. Wu, C. Dong, H. Yang, and F. Sun, "Isogeometric symmetric FE-BE coupling method for acoustic-structural interaction," *Applied Mathematics and Computation*, vol. 393, p. 125758, 2021.
- [4] L. Placidi, G. Rosi, I. Giorgio, and A. Madeo, "Reflection and transmission of plane waves at surfaces carrying material properties and embedded in second-gradient materials," *Mathematics and Mechanics of Solids*, vol. 19, no. 5, pp. 555-578, 2014.
- [5] B. L. Sharma and V. A. Eremeyev, "Wave transmission across surface interfaces in lattice structures," *International Journal of Engineering Science*, vol. 145, p. 103173, 2019.
- [6] F. Alshaikh, "Generalized thermoelastic interaction in an isotropic solid cylinder without energy dissipation," *IOP Conference Series: Materials Science and Engineering*, vol. 348, no. 1, p. 012019, 2018/04/01 2018.
- [7] O. O. Fadodun, O. G. Fadodun, A. S. Borokinni, B. A. Olokuntoye, O. P. Layeni, and A. P. Akinola, "Electroelastic constitutive model for dielectric semilinear hyperelastic solids with application to radial deformation of a rotating tube," *Meccanica*, vol. 57, no. 9, pp. 2355-2363, 2022/09/01 2022.
- [8] P. Kumar, A. Chattopadhyay, M. Mahanty, and A. K. Singh, "Analysis on propagation characteristics of the shear wave in a triple layered concentric infinite long cylindrical structure: An analytical approach," *The European Physical Journal Plus*, vol. 134, no. 1, p. 35, 2019/01/22 2019.
- [9] H. Reda, N. Karathanasopoulos, K. Elnady, J. Ganghoffer, and H. Lakiss, "Mechanics of metamaterials: an overview of recent developments," *Advances in Mechanics of Microstructured Media and Structures*, pp. 273-296, 2018.
- [10] C. Mei *et al.*, "A nonlocality-based homogenization method for dynamics of metamaterials," *Composite Structures*, p. 115716, 2022.
- [11] E. Barchiesi, M. Spagnuolo, and L. Placidi, "Mechanical metamaterials: a state of the art," *Mathematics and Mechanics of Solids*, vol. 24, no. 1, pp. 212-234, 2019.
- [12] M. Cianferra, V. Armenio, and S. Ianniello, "Hydroacoustic noise from different geometries," *International Journal of Heat and Fluid Flow*, vol. 70, pp. 348-362, 2018.
- [13] D. Borelli, T. Gaggero, E. Rizzuto, and C. Schenone, "Onboard ship noise: Acoustic comfort in cabins," *Applied Acoustics*, vol. 177, p. 107912, 2021.
- [14] R. Natarajan and A. Acrivos, "The instability of the steady flow past spheres and disks," *Journal of Fluid Mechanics*, vol. 254, pp. 323-344, 1993.
- [15] M. S. M. Ali, C. J. Doolan, and V. Wheatley, "The sound generated by a square cylinder with a splitter plate at low Reynolds number," *Journal of sound and vibration*, vol. 330, no. 15, pp. 3620-3635, 2011.

- [16] D. Jia, Y. Zou, F. Pang, X. Miao, and H. Li, "Experimental study on the characteristics of flow-induced structure noise of the underwater vehicle," *Ocean Engineering*, vol. 262, p. 112126, 2022.
- [17] D. S. Little, J. Majdalani, R. J. Hartfield Jr, and V. Ahuja, "On the prediction of noise generated by urban air mobility (UAM) vehicles. I. Integration of fundamental acoustic metrics," *Physics of Fluids*, vol. 34, no. 11, p. 116117, 2022.
- [18] X. Chen and K. R. Sreenivasan, "Reynolds number scaling of the peak turbulence intensity in wall flows," *Journal of Fluid Mechanics*, vol. 908, 2021.
- [19] A. A. Oberai, F. Roknaldin, and T. J. Hughes, "Computational procedures for determining structural-acoustic response due to hydrodynamic sources," *Computer Methods in Applied Mechanics and Engineering*, vol. 190, no. 3-4, pp. 345-361, 2000.
- [20] M. J. Lighthill, "On sound generated aerodynamically II. Turbulence as a source of sound," *Proceedings of the Royal Society of London. Series A. Mathematical and Physical Sciences*, vol. 222, no. 1148, pp. 1-32, 1954.
- [21] M. Kaltenbacher, M. Escobar, S. Becker, and I. Ali, "Numerical simulation of flow-induced noise using LES/SAS and Lighthill's acoustic analogy," *International journal for numerical methods in fluids*, vol. 63, no. 9, pp. 1103-1122, 2010.
- [22] N. Curle, "The influence of solid boundaries upon aerodynamic sound," *Proceedings of the Royal Society of London. Series A. Mathematical and Physical Sciences*, vol. 231, no. 1187, pp. 505-514, 1955.
- [23] J. E. Ffowcs Williams and D. L. Hawkings, "Sound generation by turbulence and surfaces in arbitrary motion," *Philosophical Transactions of the Royal Society of London. Series A, Mathematical and Physical Sciences*, vol. 264, no. 1151, pp. 321-342, 1969.
- [24] M. Howe, "Contributions to the theory of aerodynamic sound, with application to excess jet noise and the theory of the flute," *Journal of Fluid Mechanics*, vol. 71, no. 4, pp. 625-673, 1975.
- [25] G. MacGregor, H. Ribner, and H. Lam, "'Basic" jet noise patterns after deletion of convection and refraction effects: Experiments vs. Theory," *Journal of Sound and Vibration*, vol. 27, no. 4, pp. 437-454, 1973.
- [26] J. B. Gilbert, M. S. Howe, and R. M. Koch, "On sound generated by gas-jet impingement on a bubbly gas-water interface, with application to supercavity self-noise," *Journal of Sound and Vibration*, vol. 331, no. 20, pp. 4438-4447, 2012/09/24/ 2012.
- [27] W. Möhring, "Sound radiation by two elliptic vortex rings," *Journal of sound and vibration*, vol. 140, no. 1, pp. 155-162, 1990.
- [28] M. Goldstein and P. Ricco, "Non-localized boundary layer instabilities resulting from leading edge receptivity at moderate supersonic Mach numbers," *Journal of Fluid Mechanics*, vol. 838, pp. 435-477, 2018.
- [29] D. Terakado *et al.*, "Sound source characteristics generated by shocklets in isotropic compressible turbulence," *Physical Review Fluids*, vol. 7, no. 8, p. 084605, 2022.
- [30] F. Mao, L. Kang, L. Liu, and J. Wu, "A unified theory for gas dynamics and aeroacoustics in viscous compressible flows. Part I. Unbounded fluid," *Acta Mechanica Sinica*, vol. 38, no. 7, pp. 1-15, 2022.
- [31] C. Bailly, C. Bogey, and O. Marsden, "Progress in direct noise computation," *International Journal of Aeroacoustics*, vol. 9, no. 1-2, pp. 123-143, 2010.

- [32] M. O. Cetin, S. R. Koh, M. Meinke, and W. Schröder, "Numerical analysis of the impact of the interior nozzle geometry on low Mach number jet acoustics," *Flow, Turbulence and Combustion*, vol. 98, no. 2, pp. 417-443, 2017.
- [33] G. Romani, E. Grande, F. Avallone, D. Ragni, and D. Casalino, "Performance and noise prediction of low-Reynolds number propellers using the lattice-Boltzmann method," *Aerospace Science and Technology*, vol. 125, p. 107086, 2022.
- [34] Y. Fukushima, D. Sasaki, and K. Nakahashi, "Cartesian mesh linearized Euler equations solver for aeroacoustic problems around full aircraft," *International Journal of Aerospace Engineering*, vol. 2015, 2015.
- [35] R. Ewert and W. Schröder, "Acoustic perturbation equations based on flow decomposition via source filtering," *Journal of Computational Physics*, vol. 188, no. 2, pp. 365-398, 2003.
- [36] J. Hardin and D. Pope, "An acoustic/viscous splitting technique for computational aeroacoustics," *Theoretical and computational fluid dynamics*, vol. 6, no. 5, pp. 323-340, 1994.
- [37] W. Z. Shen, J. A. Michelsen, and J. N. Sørensen, "A collocated grid finite volume method for aeroacoustic computations of low-speed flows," *Journal of Computational Physics*, vol. 196, no. 1, pp. 348-366, 2004.
- [38] S. A. Slimon, M. C. Soteriou, and D. W. Davis, "Development of computational aeroacoustics equations for subsonic flows using a Mach number expansion approach," *Journal of Computational Physics*, vol. 159, no. 2, pp. 377-406, 2000.
- [39] Y. Bae and Y. J. Moon, "Computation of phonation aeroacoustics by an INS/PCE splitting method," *Computers & fluids*, vol. 37, no. 10, pp. 1332-1343, 2008.
- [40] J. H. Seo and Y. J. Moon, "Linearized perturbed compressible equations for low Mach number aeroacoustics," *Journal of Computational Physics*, vol. 218, no. 2, pp. 702-719, 2006.
- [41] A. Hüppe, J. Grabinger, M. Kaltenbacher, A. Reppenhagen, G. Dutzler, and W. Kühnel, "A non-conforming finite element method for computational aeroacoustics in rotating systems," in *20th AIAA/CEAS aeroacoustics conference*, 2014, p. 2739.
- [42] J. Dürrwächter, F. Meyer, T. Kuhn, A. Beck, C.-D. Munz, and C. Rohde, "A high-order stochastic Galerkin code for the compressible Euler and Navier-Stokes equations," *Computers & Fluids*, vol. 228, p. 105039, 2021/10/15/ 2021.
- [43] W. D. Roeck and W. Desmet, "Accurate CAA-Simulations Using a Low-Mach Aerodynamic/Acoustic Splitting Technique," in *15th AIAA/CEAS Aeroacoustics Conference (30th AIAA Aeroacoustics Conference)*.
- [44] C. D. Argyropoulos and N. C. Markatos, "Recent advances on the numerical modelling of turbulent flows," *Applied Mathematical Modelling*, vol. 39, no. 2, pp. 693-732, 2015/01/15/ 2015.
- [45] D. Drikakis and T. Dbouk, "The Role of Computational Science in Wind and Solar Energy: A Critical Review," *Energies*, vol. 15, no. 24, p. 9609, 2022.
- [46] G. Cao, L. Pan, and K. Xu, "High-order gas-kinetic scheme with parallel computation for direct numerical simulation of turbulent flows," *Journal of Computational Physics*, vol. 448, p. 110739, 2022.
- [47] R. Tosi, M. Núñez, J. Pons-Prats, J. Principe, and R. Rossi, "On the use of ensemble averaging techniques to accelerate the Uncertainty Quantification of CFD predictions in wind engineering," *Journal of Wind Engineering and Industrial Aerodynamics*, vol. 228, p. 105105, 2022.

- [48] J. Teng, Z. Yuan, and J. Wang, "Subgrid-scale modelling using deconvolutional artificial neural networks in large eddy simulations of chemically reacting compressible turbulence," *International Journal of Heat and Fluid Flow*, vol. 96, p. 109000, 2022.
- [49] Y. Ma, Z.-G. Yan, H. Liu, Y. Min, and H. Zhu, "Improved weighted compact nonlinear scheme for implicit large-eddy simulations," *Computers & Fluids*, vol. 240, p. 105412, 2022.
- [50] Y. Feng, F. S. Schraner, J. Winter, and N. A. Adams, "A multi-objective Bayesian optimization environment for systematic design of numerical schemes for compressible flow," *Journal of Computational Physics*, vol. 468, p. 111477, 2022.
- [51] B. Xie, F. Gao, J. Boudet, L. Shao, and L. Lu, "Improved vortex method for large-eddy simulation inflow generation," *Computers & Fluids*, vol. 168, pp. 87-100, 2018/05/30/ 2018.
- [52] GenWu, LeFang, and JinZhang, "Numerical investigation and parametric analysis of an attached eddy model applied to inlet condition," *Physics of Fluids*, vol. 34, no. 11, p. 115143, 2022.
- [53] L. Kong *et al.*, "Numerical Analysis on the Hydraulic Thrust and Dynamic Response Characteristics of a Turbine Pump," *Energies*, vol. 15, no. 4, p. 1580, 2022.
- [54] M. Harrison, W. Batten, L. Myers, and A. Bahaj, "Comparison between CFD simulations and experiments for predicting the far wake of horizontal axis tidal turbines," *IET Renewable Power Generation*, vol. 4, no. 6, pp. 613-627, 2010.
- [55] L. Kang and T. van Hooff, "Influence of inlet boundary conditions on 3D steady RANS simulations of non-isothermal mechanical ventilation in a generic closure," *International Journal of Thermal Sciences*, vol. 182, p. 107792, 2022.
- [56] A. S. Anthony, H. N. Singh, and T. N. Verma, "Computation of turbulent natural convection in an enclosure with differential flux models," *International Journal of Heat and Mass Transfer*, vol. 202, p. 123659, 2023.
- [57] K. Tawackolian and M. Kriegel, "Turbulence model performance for ventilation components pressure losses," in *Building Simulation*, 2022, vol. 15, no. 3, pp. 389-399: Springer.
- [58] P. A. Durbin, "Near-wall turbulence closure modeling without "damping functions"," *Theoretical and computational fluid dynamics*, vol. 3, no. 1, pp. 1-13, 1991.
- [59] X.-H. Zhou, J. Han, and H. Xiao, "Frame-independent vector-cloud neural network for nonlocal constitutive modeling on arbitrary grids," *Computer Methods in Applied Mechanics and Engineering*, vol. 388, p. 114211, 2022.
- [60] X. Yang, Z. Liao, and L. Yang, "Assessment of Two Streamline Curvature Correction Methods for an Elliptic Blending Turbulence Model," *Applied Sciences*, vol. 12, no. 15, p. 7899, 2022.
- [61] Y. Wang, L. Cao, Z. Cheng, B. Blanpain, and M. Guo, "Mathematical Methodology and Metallurgical Application of Turbulence Modelling: A Review," *Metals*, vol. 11, no. 8, p. 1297, 2021.
- [62] J. W. Kim and R. D. Sandberg, "Efficient parallel computing with a compact finite difference scheme," *Computers & Fluids*, vol. 58, pp. 70-87, 2012/04/15/ 2012.
- [63] G. Alfonsi, S. A. Ciliberti, M. Mancini, and L. Primavera, "Direct Numerical Simulation of Turbulent Channel Flow on High-Performance GPU Computing System," *Computation*, vol. 4, no. 1, p. 13, 2016.

- [64] G. Alfonsi, S. A. Ciliberti, M. Mancini, and L. Primavera, "GPGPU implementation of mixed spectral-finite difference computational code for the numerical integration of the three-dimensional time-dependent incompressible Navier–Stokes equations," *Computers & Fluids*, vol. 102, pp. 237-249, 2014/10/10/ 2014.
- [65] S. Laizet, E. Lamballais, and J. C. Vassilicos, "A numerical strategy to combine high-order schemes, complex geometry and parallel computing for high resolution DNS of fractal generated turbulence," *Computers & Fluids*, vol. 39, no. 3, pp. 471-484, 2010/03/01/ 2010.
- [66] P. R. Spalart and C. Streett, "Young-person's guide to detached-eddy simulation grids," 2001.
- [67] L. Deng, Y. Long, and B. Ji, "Delayed detached eddy simulation and vorticity analysis of cavitating flow around a marine propeller behind the hull," *Ocean Engineering*, vol. 264, p. 112442, 2022.
- [68] G. Chen, X.-B. Li, and X.-F. Liang, "IDDES simulation of the performance and wake dynamics of the wind turbines under different turbulent inflow conditions," *Energy*, vol. 238, p. 121772, 2022.
- [69] H. Guo, G. Li, and Z. Zou, "Numerical Simulation of the Flow around NACA0018 Airfoil at High Incidences by Using RANS and DES Methods," *Journal of Marine Science and Engineering*, vol. 10, no. 7, p. 847, 2022.
- [70] V. Markov, B. Sa, V. Kamaltdinov, V Neverov and A Zherdev, "Investigation on the effect of the flow passage geometry of diesel injector nozzle on injection process parameters and engine performances," vol.10, pp. 552-577,2022.
- [71] A. Sohankar, "Large eddy simulation of flow past rectangular-section cylinders: Side ratio effects," *Journal of Wind Engineering and Industrial Aerodynamics*, vol. 96, no. 5, pp. 640-655, 2008/05/01/ 2008.
- [72] N. Papaxanthos, E. Perrey-Debain, S. Bennouna, B. Ouedraogo, S. Moreau, and J.-M. Ville, "Pressure-based integral formulations of Lighthill–Curlle's analogy for internal aeroacoustics at low Mach numbers," *Journal of Sound and Vibration*, vol. 393, pp. 176-186, 2017.
- [73] C. Zhang, M. Sanjose, and S. Moreau, "Aeolian noise of a cylinder in the critical regime," *The Journal of the Acoustical Society of America*, vol. 146, no. 2, pp. 1404-1415, 2019.
- [74] R. Porteous, D. J. Moreau, and C. J. Doolan, "The aeroacoustics of finite wall-mounted square cylinders," *Journal of Fluid Mechanics*, vol. 832, pp. 287-328, 2017.
- [75] D. J. Moreau and C. J. Doolan, "Flow-induced sound of wall-mounted finite length cylinders," *AIAA journal*, vol. 51, no. 10, pp. 2493-2502, 2013.
- [76] Y. Wang, D. Thompson, and Z. Hu, "Numerical investigations on the flow over cuboids with different aspect ratios and the emitted noise," *Physics of Fluids*, vol. 32, no. 2, p. 025103, 2020.
- [77] P. Bearman and D. Trueman, "An investigation of the flow around rectangular cylinders," *Aeronautical Quarterly*, vol. 23, no. 3, pp. 229-237, 1972.
- [78] W.-S. Choi, Y. Choi, S.-Y. Hong, J.-H. Song, H.-W. Kwon, and C.-M. Jung, "Turbulence-induced noise of a submerged cylinder using a permeable FW–H method," *International Journal of Naval Architecture and Ocean Engineering*, vol. 8, no. 3, pp. 235-242, 2016.
- [79] M. Cianferra, S. Ianniello, and V. Armenio, "Assessment of methodologies for the solution of the Ffowcs Williams and Hawkings equation using LES of incompressible single-phase flow around a finite-size square cylinder," *Journal of Sound and Vibration*, vol. 453, pp. 1-24, 2019.

- [80] P. Bathla and J. Kennedy, "3D printed structured porous treatments for flow control around a circular cylinder," *Fluids*, vol. 5, no. 3, p. 136, 2020.
- [81] S. Bulut and S. Ergin, "Effects of temperature, salinity, and fluid type on acoustic characteristics of turbulent flow around circular cylinder," *Journal of Marine Science and Application*, vol. 20, no. 2, pp. 213-228, 2021.
- [82] A. K. Lidtke, M. Klapwijk, and T. Lloyd, "Scale-resolving simulations of a circular cylinder subjected to low mach number turbulent inflow," *Journal of Marine Science and Engineering*, vol. 9, no. 11, p. 1274, 2021.
- [83] S. Bulut and S. Ergin, "Numerical investigation of geometrical parameters on the hydrodynamic noise characteristics of submerged bodies and comparisons with experiments," *Proceedings of the Institution of Mechanical Engineers, Part M: Journal of Engineering for the Maritime Environment*, vol. 235, no. 4, pp. 866-884, 2021.
- [84] B. C. Feijó, C. Fragassa, F. B. Teixeira, L. A. O. Rocha, L. A. Isoldi, and E. D. dos Santos, "Geometrical investigation of cooling channels with two alternated isothermal blocks under forced convective turbulent flow," *Continuum Mechanics and Thermodynamics*, vol. 34, no. 6, pp. 1687-1709, 2022.
- [85] M. Arif, A. Saeed, P. Suttiarporn, W. Khan, P. Kumam, and W. Wathayu, "Analysis of second grade hybrid nanofluid flow over a stretching flat plate in the presence of activation energy," *Scientific Reports*, vol. 12, no. 1, pp. 1-18, 2022.
- [86] Y. Liu, X. Sun, V. Sethi, D. Nalianda, Y.-G. Li, and L. Wang, "Review of modern low emissions combustion technologies for aero gas turbine engines," *Progress in Aerospace Sciences*, vol. 94, pp. 12-45, 2017.
- [87] R. Laohasurayodhin, P. Diloksumpan, P. Sakiyalak, and P. Naiyanetr, "Computational fluid dynamics analysis and validation of blood flow in Coronary Artery Bypass Graft using specific models," in *The 7th 2014 Biomedical Engineering International Conference*, 2014, pp. 1-4: IEEE.
- [88] K. Sukhapore, A. Burns, T. Mahmud, and J. Spooner, "Computational fluid dynamics modelling and validation of head losses in pipe bifurcations," 2017.
- [89] E. Gedik, "Experimental and numerical Investigation on laminar pipe flow of magnetorheological fluids under applied external magnetic field," *Journal of Applied Fluid Mechanics*, vol. 10, no. 3, pp. 801-811, 2017.
- [90] T. Patel, S. Singh, and V. Seshadri, "Characteristics of Y-shaped rectangular diffusing duct at different inflow conditions," *Journal of aircraft*, vol. 42, no. 1, pp. 113-120, 2005.
- [91] Y. Zhang, Y. Bazilevs, S. Goswami, C. L. Bajaj, and T. J. Hughes, "Patient-specific vascular NURBS modeling for isogeometric analysis of blood flow," *Computer methods in applied mechanics and engineering*, vol. 196, no. 29-30, pp. 2943-2959, 2007.
- [92] A. B. Desamala, A. K. Dasamahapatra, and T. K. Mandal, "Oil-water two-phase flow characteristics in horizontal pipeline—a comprehensive CFD study," *International journal of Chemical, Molecular, Nuclear, Materials and Metallurgical Engineering, World Academy of Science, Engineering and Technology*, vol. 8, no. 4, pp. 360-364, 2014.
- [93] N. M. Martins, N. J. Carriço, H. M. Ramos, and D. I. Covas, "Velocity-distribution in pressurized pipe flow using CFD: Accuracy and mesh analysis," *Computers & Fluids*, vol. 105, pp. 218-230, 2014.
- [94] J. O. de Brito Lira, H. G. Riella, N. Padoin, and C. Soares, "Fluid dynamics and mass transfer in curved reactors: A CFD study on Dean flow effects," *Journal of Environmental Chemical Engineering*, vol. 10, no. 5, p. 108304, 2022.

- [95] V. Kumar, "Simulation and flow analysis through different pipe geometry," 2014.
- [96] Y. Wang, K. Su, H.-g. Wu, and Z.-d. Qian, "Flow characteristics of large hydropower bifurcation under structure rounding optimization," *International Journal of Civil Engineering*, vol. 15, no. 4, pp. 515-529, 2017.
- [97] E. Massoud, Q. Xiao, H. El-Gamal, and M. Teamah, "Numerical study of an individual Taylor bubble rising through stagnant liquids under laminar flow regime," *Ocean Engineering*, vol. 162, pp. 117-137, 2018.
- [98] B. B. Nayak and D. Chatterjee, "Convective heat transfer in slurry flow in a horizontal Y-shaped branch pipe," *Powder technology*, vol. 318, pp. 46-61, 2017.
- [99] X. Li and S. Wang, "Flow field and pressure loss analysis of junction and its structure optimization of aircraft hydraulic pipe system," *Chinese Journal of Aeronautics*, vol. 26, no. 4, pp. 1080-1092, 2013.
- [100] C. Cornelius, T. Biesinger, P. Galpin, and A. Braune, "Experimental and computational analysis of a multistage axial compressor including stall prediction by steady and transient CFD methods," *Journal of Turbomachinery*, vol. 136, no. 6, p. 061013, 2014.
- [101] H. A. Mrope, Y. A. Chande Jande, and T. T. Kivevele, "A Review on Computational Fluid Dynamics Applications in the Design and Optimization of Crossflow Hydro Turbines," *Journal of Renewable Energy*, vol. 2021, 2021.
- [102] Y. Zou, X. Zhao, and Q. Chen, "Comparison of STAR-CCM+ and ANSYS Fluent for simulating indoor airflows," in *Building simulation*, 2018, vol. 11, no. 1, pp. 165-174: Springer.
- [103] S. Chen, B. Du, Q. Li, and D. Xue, "The influence of different orientations and ventilation cases on temperature distribution of the car cabin in the hot soak," *Case Studies in Thermal Engineering*, vol. 39, p. 102401, 2022/11/01/ 2022.
- [104] O. Marfaing *et al.*, "Comparison and uncertainty quantification of two-fluid models for bubbly flows with NEPTUNE_CFD and STAR-CCM+," *Nuclear Engineering and Design*, vol. 337, pp. 1-16, 2018/10/01/ 2018.
- [105] L. Chen, C. Huang, and C. Xu, "A farmers market architecture and ventilation design and its airflow analysis," *International Journal of Ventilation*, pp. 1-21, 2021.
- [106] J. Liu, S. Zhu, M. K. Kim, and J. Srebric, "A review of CFD analysis methods for personalized ventilation (PV) in indoor built environments," *Sustainability*, vol. 11, no. 15, p. 4166, 2019.
- [107] T. Dai, S. Liu, J. Liu, N. Jiang, W. Liu, and Q. Chen, "Evaluation of fast fluid dynamics with different turbulence models for predicting outdoor airflow and pollutant dispersion," *Sustainable Cities and Society*, vol. 77, p. 103583, 2022.
- [108] B. Zang, V. Us, H. D. Lim, X. Wei, and T. H. New, "An assessment of OpenFOAM solver on RANS simulations of round supersonic free jets," *Journal of Computational Science*, vol. 28, pp. 18-31, 2018/09/01/ 2018.
- [109] V. Zmijanovic, L. Leger, M. Sellam, and A. Chpoun, "Assessment of transition regimes in a dual-bell nozzle and possibility of active fluidic control," *Aerospace Science and Technology*, vol. 82-83, pp. 1-8, 2018/11/01/ 2018.
- [110] V. Seidl, S. Muzaferija, and M. Perić, "Parallel DNS with Local Grid Refinement," *Applied Scientific Research*, vol. 59, no. 4, pp. 379-394, 1997/12/01 1997.
- [111] H. J. Kim and P. A. Durbin, "Observations of the frequencies in a sphere wake and of drag increase by acoustic excitation," *The Physics of Fluids*, vol. 31, no. 11, pp. 3260-3265, 1988.

- [112] A. Posa, R. Broglia, M. Felli, M. Cianferra, and V. Armenio, "Hydroacoustic analysis of a marine propeller using large-eddy simulation and acoustic analogy," *Journal of Fluid Mechanics*, vol. 947, p. A46, 2022.
- [113] B. Cantwell and D. Coles, "An experimental study of entrainment and transport in the turbulent near wake of a circular cylinder," *Journal of fluid mechanics*, vol. 136, pp. 321-374, 1983.
- [114] C. Norberg, "Fluctuating lift on a circular cylinder: review and new measurements," *Journal of Fluids and Structures*, vol. 17, no. 1, pp. 57-96, 2003.
- [115] R. Abdi, N. Rezazadeh, and M. Abdi, "Investigation of passive oscillations of flexible splitter plates attached to a circular cylinder," *Journal of Fluids and Structures*, vol. 84, pp. 302-317, 2019.
- [116] M. Prsic, M. C. Ong, B. Pettersen, and D. Myrhaug, "Large eddy simulations of three-dimensional flow around a pipeline in a uniform current," in *International Conference on Offshore Mechanics and Arctic Engineering*, 2012, vol. 44922, pp. 539-548: American Society of Mechanical Engineers.
- [117] R. Orselli, J. Meneghini, and F. Saltara, "Two and three-dimensional simulation of sound generated by flow around a circular cylinder," in *15th AIAA/CEAS aeroacoustics conference (30th AIAA aeroacoustics conference)*, 2009, p. 3270.
- [118] C.-W. Park and S.-J. Lee, "Flow structure around a finite circular cylinder embedded in various atmospheric boundary layers," *Fluid Dynamics Research*, vol. 30, no. 4, p. 197, 2002.
- [119] M. Breuer, "Large eddy simulation of the subcritical flow past a circular cylinder: numerical and modeling aspects," *International journal for numerical methods in fluids*, vol. 28, no. 9, pp. 1281-1302, 1998.
- [120] D. A. Lysenko, I. S. Ertesvåg, and K. E. Rian, "Large-eddy simulation of the flow over a circular cylinder at Reynolds number 3900 using the OpenFOAM toolbox," *Flow, turbulence and combustion*, vol. 89, no. 4, pp. 491-518, 2012.
- [121] J. Franke and W. Frank, "Large eddy simulation of the flow past a circular cylinder at $Re_D = 3900$," *Journal of wind engineering and industrial aerodynamics*, vol. 90, no. 10, pp. 1191-1206, 2002.
- [122] X. Du, H. Cui, and Z. Zhang, "A numerical method for analyzing the influence of underwater vehicle flow field on dynamic behavior of towed sonar cable array," *Ocean Engineering*, vol. 175, pp. 163-175, 2019.
- [123] "Defense Technical Information Center," Dtic.mil, 2024. [https:// apps. dtic.mil/ sti/citations /tr/ ADA359226](https://apps.dtic.mil/sti/citations/tr/ADA359226) (accessed Mar. 16, 2024).
- [124] H. Yao, H. Zhang, H. Liu, and W. Jiang, "Numerical study of flow-excited noise of a submarine with full appendages considering fluid structure interaction using the boundary element method," *Engineering Analysis with Boundary Elements*, vol.77,pp.1–9, Apr. 2017, doi: <https://doi.org/10.1016/j.enganabound.2016.12.012>.
- [125] K Karthik, S Jeyakumar, and J Sarathkumar Sebastin, "Numerical prediction of flow noise levels on towed sonar array," *Proceedings of the Institution of Mechanical Engineers, Part M: Journal of Engineering for the Maritime Environment*, vol. 235, no. 2, pp. 600–606, Oct. 2020, doi: <https://doi.org/10.1177/1475090220961922>.